

ICE RUBBLE ACCUMULATION EVENT ANALYSIS:
LEVEL ICE INTERACTION WITH UPWARD
BREAKING CONICAL STRUCTURES

CENTRE FOR NEWFOUNDLAND STUDIES

**TOTAL OF 10 PAGES ONLY
MAY BE XEROXED**

(Without Author's Permission)

SUSAN PFISTER



NOTE TO USERS

This reproduction is the best copy available.

UMI[®]

**Ice Rubble Accumulation Event Analysis: Level Ice Interaction With
Upward Breaking Conical Structures**

by Susan Pfister, B.Sc. E.

A thesis submitted to the School of Graduate Studies in
partial fulfillment of the requirements for the degree of
Master's of Ocean Engineering

Faculty of Engineering and Applied Science
Memorial University of Newfoundland
August, 2004

St. John's

Newfoundland

Canada



Library and
Archives Canada

Bibliothèque et
Archives Canada

Published Heritage
Branch

Direction du
Patrimoine de l'édition

395 Wellington Street
Ottawa ON K1A 0N4
Canada

395, rue Wellington
Ottawa ON K1A 0N4
Canada

Your file *Votre référence*

ISBN: 0-494-02369-4

Our file *Notre référence*

ISBN: 0-494-02369-4

NOTICE:

The author has granted a non-exclusive license allowing Library and Archives Canada to reproduce, publish, archive, preserve, conserve, communicate to the public by telecommunication or on the Internet, loan, distribute and sell theses worldwide, for commercial or non-commercial purposes, in microform, paper, electronic and/or any other formats.

The author retains copyright ownership and moral rights in this thesis. Neither the thesis nor substantial extracts from it may be printed or otherwise reproduced without the author's permission.

AVIS:

L'auteur a accordé une licence non exclusive permettant à la Bibliothèque et Archives Canada de reproduire, publier, archiver, sauvegarder, conserver, transmettre au public par télécommunication ou par l'Internet, prêter, distribuer et vendre des thèses partout dans le monde, à des fins commerciales ou autres, sur support microforme, papier, électronique et/ou autres formats.

L'auteur conserve la propriété du droit d'auteur et des droits moraux qui protègent cette thèse. Ni la thèse ni des extraits substantiels de celle-ci ne doivent être imprimés ou autrement reproduits sans son autorisation.

In compliance with the Canadian Privacy Act some supporting forms may have been removed from this thesis.

Conformément à la loi canadienne sur la protection de la vie privée, quelques formulaires secondaires ont été enlevés de cette thèse.

While these forms may be included in the document page count, their removal does not represent any loss of content from the thesis.

Bien que ces formulaires aient inclus dans la pagination, il n'y aura aucun contenu manquant.


Canada

Abstract

Incidents of ice rubble accumulation are associated with force maxima in field observations and therefore the understanding of ice rubble processes is desirable for the purposes of determining design loads for offshore structures. In 1999, a series of tests to observe level ice interacting with upward breaking conical structures was conducted in C-CORE's geotechnical centrifuge. A complementary test series was conducted at IMD's ice tank in 2000. A field program to obtain ice observations was carried out in the spring of 2001 at the Confederation Bridge. Data from these three sources was examined in the context of friction, fracture mechanics, and dimensional analysis. A minimum energy approach has been found to be most useful in predicting the combination of variables which will result in ice rubble accumulation. The ratio of force to fail an ice floe locally (rubbling) versus the force to fail an ice floe globally (splitting) is investigated as a practical method of comparison of data from different scales.

Acknowledgments

This work would not even have begun without the mention of an interesting talk by my good friend Marie Wardman, nor without the patience of Paul Barette in answering a seemingly endless barrage of questions about C-CORE/MUN and life in Newfoundland.

Special thanks is due to my supervisors, Dr. Ryan Phillips and Dr. F. Mary Williams for their support and encouragement. I appreciate having had the chance to work with both of you. Getting to PEI and seeing things happening was pivotal – many thanks to Derek Mayne and Dr. Tom Brown for the opportunity. Dr. Michael Lau gave generously of his time and expertise. Thanks also to everyone who helped with the various technical aspects of my research – Don, Austin, Brian, and others. Thanks to the Sid Blair Foundation for the opportunity to travel to the 16th International IAHR Ice Symposium.

And lastly thanks to my family for tolerating such a hare-brained scheme as more school after four short years of undergrad, and to my friends both in Newfoundland and beyond for listening, empathizing, and prodding. Cha Gheill!

TABLE OF CONTENTS

Abstract.....	ii
Acknowledgements.....	iii
LIST OF TABLES.....	vi
LIST OF FIGURES.....	vii
LIST OF APPENDICES.....	viii
1 INTRODUCTION.....	1
1.1 PROTOTYPE CASE.....	2
1.2 MODELLING PROGRAMS.....	3
1.3 PURPOSE OF THE PROJECT.....	3
2 LITERATURE REVIEW.....	5
2.1 ICE AND ICE RUBBLE.....	5
2.1.1 Definition of ice.....	5
2.1.2 Crystal Structure and Factors Influencing Mechanical Properties.....	5
2.1.3 Ice Types and Sea Ice Classification.....	7
2.1.4 Properties and Materials Testing Procedures.....	9
2.1.4.1 Testing of Ice beams.....	9
2.1.4.2 Flexural Strength of Ice.....	10
2.1.4.3 Compressive Strength of Ice.....	11
2.1.4.4 Flexural Strength Compared to Compressive Strength of Ice.....	11
2.1.5 Rubble Pile Definition.....	12
2.1.6 Force Models for Ice Loads on Structures.....	14
2.1.6.1 Croasdale’s Ice Force Model.....	15
2.1.6.2 Nevel’s Ice Force Model.....	16
2.1.6.3 Shear Failure of Level Ice.....	17
2.1.7 Previous Rubble Pile Observations.....	18
2.2 PROTOTYPE CONDITIONS – THE CONFEDERATION BRIDGE.....	20
2.2.1 Ice Rubble Accumulation at the Confederation Bridge.....	22
2.3 CENTRIFUGE MODELLING.....	24
2.4 IMD TEST SERIES.....	28
2.5 FRICTION AND ICE-STRUCTURE INTERACTION.....	29
2.6 FRACTURE MECHANICS AND ICE-STRUCTURE INTERACTION.....	34
2.7 DIMENSIONAL ANALYSIS.....	36
3 EXPERIMENTAL METHODS.....	40
3.1 CENTRIFUGE DATA.....	40
3.1.1 Rubble accumulation analysis: selection of method.....	43
3.1.2 Thin sectioning of centrifuge rubble accumulations.....	45
3.2 ICE TANK DATA.....	48
3.3 PROTOTYPE DATA.....	51
3.3.1 Field data collection: selection of method.....	54
3.3.2 Field data: video analysis.....	55
4 EXPERIMENTAL RESULTS.....	58
4.1 CENTRIFUGE DATA.....	58

4.1.1	Qualitative observations – video.....	58
4.1.2	Quantitative observations – thin sections	59
4.1.3	Thin section method – data considerations.....	64
4.1.4	Thin section observations – discussion.....	66
4.2	ICE TANK DATA.....	66
4.2.1	Qualitative observations – process description.....	67
4.3	PROTOTYPE DATA	67
4.3.1	Qualitative observations – process description.....	67
4.3.2	Quantitative observations.....	72
4.3.3	Field observations – discussion	72
5	DISCUSSION.....	77
5.1	COMPARISON OF FIELD AND MODEL OBSERVATIONS	77
5.1.1	Field and ice tank observations.....	77
5.1.2	Ice tank and centrifuge observations.....	77
5.1.2.1	Freshwater centrifuge tests and ice tank tests	77
5.1.2.2	Saline centrifuge tests and ice tank tests.....	78
5.1.3	Field and freshwater centrifuge observations	78
5.1.4	Comparison of physical observations with numerical model assumptions.....	79
5.2	FRICITION BASED ANALYSIS OF ICE RUBBLE ACCUMULATION	80
5.3	FRACTURE MECHANICS APPLIED TO ICE RUBBLE ACCUMULATION.....	81
5.4	DIMENSIONAL ANALYSIS APPLIED TO ICE-RUBBLE ACCUMULATION	86
5.4.1	Development of Model	86
5.4.2	Ice Rubble Accumulation Cases	89
5.4.2.1	Prototype	89
5.4.2.2	Ice Tank	92
5.4.2.3	Centrifuge	94
5.4.3	Model Results	96
5.4.4	Implications.....	102
5.5	FRACTURE MECHANICS AND DIMENSIONAL ANALYSIS	102
6	CONCLUSIONS.....	105
7	REFERENCES	108

LIST OF TABLES

Table 2. 1: Ice Properties in the Northumberland Strait.	21
Table 2. 2: Minimum friction coefficients for ice rubble accumulation.....	33
Table 3. 1:Ice Properties in the Northumberland Strait.	21
Table 3. 2: Minimum friction coefficients for ice rubble accumulation.....	33
Table 3. 3: Centrifuge test series summary.....	43
Table 3. 4: Labelling scheme for thin sections	48
Table 3. 5: IMD test series summary	50
Table 3. 6: Prototype non-rubbling events observed during field program, spring 2001. 52	
Table 3. 7: Prototype rubbing events observed during field program, spring 2001.	54
Table 4. 1: Centrifuge thin section properties.....	61
Table 5. 1: Material properties of ice.....	84
Table 5. 2: Rubble Pile Formation Factors.	87
Table 5. 3: Variable values for prototype conditions.....	91
Table 5. 4: Values of Π terms for prototype rubbing conditions.....	91
Table 5. 5: Values of Π terms for prototype non-rubbling conditions	91
Table 5. 6: Variable values for ice tank	93
Table 5. 7: Values of Π terms for ice tank conditions (non-rubbling)	93
Table 5. 8: Variable values for centrifuge (freshwater).....	94
Table 5. 9: Variable values for centrifuge (saline)	95
Table 5. 10: Values of Π terms for centrifuge freshwater	95
Table 5. 11: Values of Π terms for centrifuge saline.....	95
Table 5. 12: Froude comparison, all test cases	96
Table 5. 13: Ratio of critical to actual radii, all model conditions.....	103

LIST OF FIGURES

Figure 2. 1: Rubble pile dimensions.	13
Figure 2. 2: Principles of centrifuge modeling.	25
Figure 2. 3: Centrifuge package.....	27
Figure 3. 1: Freshwater ice rubble accumulation in the centrifuge.....	41
Figure 3. 2: Saline ice sheet deformed following interaction in the centrifuge.	42
Figure 3. 3: Illustrative sample thin section.....	46
Figure 4. 1: Crossed polar view of ICESTR32iv270dfdt.	60
Figure 4. 2: Crossed polar view of ICESTR32iii235dfdt.	62
Figure 4. 3: Crossed polar view of ICESTR33iiiptdt.	64
Figure 4. 4: Typical Confederation Bridge level ice interaction sequence.....	70
Figure 4. 5: Marker path during rubble accumulation event.	71
Figure 4. 6: Examination of video data quantified in terms of pile geometry.....	74
Figure 4. 7: Floe size versus floe velocity for field program observations.....	76
Figure 4. 8: Transition to global failure plotted relative to floe size.	76
Figure 5. 1: Aspect ratio versus fracture toughness term.....	100
Figure 5. 2: Cauchy term versus fracture toughness term.	100
Figure 5. 3: Stiffness term versus fracture toughness term.....	101
Figure 5. 4: Froude number versus fracture toughness term.	101

LIST OF APPENDICES

APPENDIX A: THIN SECTIONS FROM CENTRIFUGE TEST SERIES

LIST OF SYMBOLS

A_c	= contact area
b	= beam width
c	= cohesion
E	= Young's modulus
g	= acceleration due to gravity
h	= ice thickness
l_c	= characteristic length
M	= maximum moment resistance
N	= normal force
P	= rubble pile height
p_e	= effective ice-pressure
ppt	= parts per thousand
psu	= practical salinity units
r	= structure radius
R	= floe radius
T	= force on an object to initiate motion
V	= ice velocity
α	= angle of structure with respect to horizontal
μ	= friction co-efficient
ρ_w	= mass density of water
ρ_i	= mass density of ice
ϕ	= friction angle
σ_y	= yield strength of material
σ_f	= flexural strength of ice ($\cong \sigma_t$ for purposes of this study)
τ_m	= shear strength of material

1 INTRODUCTION

The study of sea ice has been of interest since the 18th century when the hopes of trade with the Far East influenced foreign policy in Europe. The dream of the Northwest Passage lured many ships and men to their demise in the Arctic. In many cases, their deaths resulted from poor planning, an unwillingness to change their routines to suit their new environment, and the crushing force of the ice of the polar pack. Today, with the recent discovery of economic mineral reserves in inhospitable locations such as the polar shelves, resource extraction drives the study of sea ice.

Ice-structure interaction investigates the reaction of ships, bridge piers and other anthropogenic structures to ice loads. Ice rubble forms when large ice features break against each other or against structures, creating ice pieces of various sizes. Understanding the nature of ice rubble, and the circumstances which lead to its generation and accumulation around structure, etc., is still in its infancy.

The objective of this thesis is to investigate the occurrence of ice rubble accumulation events following contact between level ice and an upward breaking conical structure. These events will be studied at two scales in detail: prototype and small scale physical models tested in a geotechnical centrifuge. Comparison will also be made with the results of a series of tests conducted in a large model ice tank. The ice tank models ice-structure interaction at a slightly reduced scale using ice with altered physical properties. The analyses of processes at three scales are conducted to determine if the centrifuge and

ice tank accurately predict the behaviour of ice at prototype scale. Ice forces are not compared in this study; however, the ultimate application of the understanding of rubble processes is to integrate these findings with ice force data to predict design conditions of offshore structures.

1.1 PROTOTYPE CASE

A better understanding of ice rubble is necessary because ice force maxima have been found to correlate with the formation of rubble piles around conical structures (Mayne and Brown, 2000). The Confederation Bridge, which spans the Northumberland Strait between New Brunswick (NB) and Prince Edward Island (PEI), Canada, has been identified as the prototype case for this study. This bridge is currently the longest in the world to span waters that are regularly ice covered.

The completion of the bridge in 1997 represents a considerable engineering achievement. It is also a unique opportunity to gather data about the processes involved in ice structure interaction. Preceding the bridge's construction, several studies were conducted to attempt to determine the potential environmental loads on the bridge. These included field programs to measure physical properties of the ice in the Northumberland Strait and experimental testing to predict the load that ice of various types would exert on the bridge piers.

1.2 MODELLING PROGRAMS

Interest in the subject of ice-structure interaction has increased since the bridge was completed. Modelling the process of ice-structure interaction is continuing at various scales and new methods of physical modelling are being investigated. A study was conducted in St. John's, NL at two different research facilities to determine the applicability of geotechnical centrifuge modelling to the study of ice-structure interaction and compare results from the centrifuge with those obtained in conventional ice testing basins between 1998 and 2002 (Barrette *et al.* 1998, 2000, Lau *et al.* 2002). The study was funded by an NRC-NSERC Research Partnership Grant and included a corresponding test series in level ice at the Institute for Marine Dynamics (IMD) in the facility's 12 m × 90 m ice tank.

1.3 PURPOSE OF THE PROJECT

This research has been conducted to better understand the combination of factors resulting in ice rubble accumulation and to apply this knowledge to prediction of ice rubble accumulation events – i.e., what combination of variables (floe size, ice velocity, ice thickness, structure geometry, etc.) results in the accumulation of a pile of small pieces of ice (ice rubble) in front of a structure in the field, centrifuge, and ice tank? Analysis is accomplished by comparison of results of the field observations with the results of the centrifuge and ice tank test series and the application of various theoretical treatments, including fracture mechanics and dimensional analysis, to these data.

The small size of ice rubble accumulations created in the centrifuge tests allowed unique observations to be collected using thin sections, which enabled the author to view the internal structure of the deformed ice sheet and associated rubble pile geometry. Thin sections showed that the process of ice rubble formation and accumulation is associated with local ice failure for freshwater centrifuge tests. In saline centrifuge tests, ice rubble accumulation was not observed, but cracking of the ice sheet occurred to accommodate movement of the ice sheet around the structure. Field observations also showed that non-rubble accumulation events are associated with floe splitting, a global failure mechanism. Short-circuiting of the rubble pile, which involves the relocation of the incoming level ice sheet within the rubble pile, was observed in the thin sections and also in the field at the Confederation Bridge. This commonality provides support for the hypothesis that the process seen in the centrifuge tests accurately replicates the rubble accumulation processes in the prototype case.

This thesis is subdivided into six chapters, including this introduction. Chapter 2 consists of a review of the relevant literature; Chapter 3 discusses methods of data gathering for the centrifuge test series and field observations; Chapter 4 provides experimental results and field observations; Chapter 5 reviews these observations in the context of friction, fracture mechanics, and dimensional analysis; and Chapter 6 states the conclusions reached from this work. References are listed in Section 7.

2 LITERATURE REVIEW

2.1 ICE AND ICE RUBBLE

2.1.1 Definition of ice

Ice is a crystalline solid composed of hydrogen and oxygen atoms. It has nine polymorphs (forms of the same chemical composition with a different crystal structure). Only one is found at average environmental temperature and pressure conditions. The others occur at high pressures in nature or are artificial products of a laboratory environment (Cammaert and Muggeridge, 1988). Ice may contain inclusions of other substances such as gas bubbles or brine, but these do not fit easily into the crystal lattice and tend to occur in localized areas. Ice is classified on the basis of its crystallization process and the nature of the water used during the freezing process. The mechanical properties of ice vary within this classification scheme; however, the following approximation can be made: its compressive strength is 1% that of steel and 10% that of concrete.

2.1.2 Crystal Structure and Factors Influencing Mechanical Properties

The crystal form of ice is hexagonal. This is exhibited in the hexagonal form of snowflakes (atmospheric ice). The formation of ice depends on a combination of circumstances. The water surface must be relatively still to allow the formation of a supercooled layer of water. “Supercooled” in this instance implies water slightly below the freezing temperature, usually approximately -0.01°C (Cammaert and Muggeridge,

1988). Only in extreme conditions where the air temperatures are between -38°C and -42°C will ice crystallization begin spontaneously. Otherwise a nucleus of some type is required to begin the process. This may consist of atmospheric ice in the form of fog or snowflakes. Once the coverage of the surface by these nuclei is laterally extensive, crystals begin to grow vertically (Cammaert and Muggeridge, 1988).

The initial seeding event and growth of the surface layer is called primary ice growth. The subsequent vertical crystal growth is referred to as secondary ice growth. As previously mentioned, ice does not accommodate irregularities in composition well. Brine becomes trapped in sea ice as it is rejected from the growing ice sheet to fill spaces between dendrites (rows of cellular projections) at the ice-water interface. As the ice sheet continues to thicken, the pockets of brine become isolated as the ice grows around them. The ice will advance until it is unable to close in further due to the high salinity of the brine solution. Brine cells are commonly approximately 0.5 mm across. Systems of such cells develop in a vertical sheet like fashion due to successive ice growth across the same void between dendrites (Wadhams, 2000). Superimposed ice grows on the surface of primary ice. It may form from water which seeps onto the surface through cracks or via the refreezing of melted ice (Cammaert and Muggeridge, 1988). Brine leaves ice sheets by various mechanisms, including brine cell migration, brine expulsion, and gravity drainage (Wadhams, 2000).

The salinity of ice can be expressed in terms of concentration (e.g. ppt) or conductivity as compared with that of a standard solution (e.g. psu). Sea ice salinity ranges from 10 psu (young sea ice) to 1-3 psu (multi year ice) (Wadhams, 2000). As saline ice ages, its composition approaches that of freshwater ice. The concentrated brine solutions in the brine pockets leave the ice sheet by two mechanisms (Cammaert and Muggeridge, 1988). The first occurs at temperatures above -15 °C, and consists of slow drainage of brine through interconnected channels. This process is fastest when ice is near its melting point. The second process is called brine cell migration and occurs over long periods of time. The temperature gradient through the ice sheet causes movement of the brine solution from the colder (usually top) to warmer (usually bottom) ice surface by partial melting and recrystallization. This means a net downward movement of brine cells toward the ice-water interface under average conditions. Ice strength increases with decreasing salinity and temperature (Williams and Parsons, 1994). Grain size is also inversely related to ice strength - ice with large grains is weaker than ice with small grains (Timco and O'Brien, 1994).

2.1.3 Ice Types and Sea Ice Classification

Ice at sea is classified both by its geographical location and by its age. Ice which has formed in the season under investigation is called first year ice. Wadhams (2000) defines ice which has survived a single summer as second year ice; ice older than this is known as old ice. Wadhams (2000) also states that any ice older than first year ice is usually

termed multi-year ice due to the difficulty associated with differentiating between ice types visually.

Sea ice is an important consideration for any project in the Arctic or the north-eastern coastal regions of Canada. First year sea ice is the most common type of ice in the areas of the Canadian Arctic which are being considered for hydrocarbon development. In first year ice, the feature of most concern is an ice ridge, an agglomeration of small ice pieces which forms most commonly through compressive or shear failure of ice sheets. Ridges are characterized by their cross section, and the proportion of ice above and below the waterline. The keel depth is the maximum depth of the ridge below the waterline and the sail height is the maximum height of the ridge above the waterline. The keel depth is typically 4.5 to 6 times greater than the sail height (Cammaert and Muggeridge, 1988). When these features are initially formed, they consist of a poorly consolidated mass of fragments held together by buoyancy, gravity, and friction. However, with the passage of time, the region of the ridge within approximately 2 metres of the waterline becomes consolidated and will become as strong as or stronger than the surrounding ice sheet (Wadhams, 2000). Consolidation of ice at the waterline occurs via processes of rafting and amalgamation of adjacent ice sheets under pressure, and results in a thickened and strengthened layer near the waterline. It is this process that makes ridges dangerous to structures in ice covered waters. There is also the additional risk of the inclusion of pieces of glacial ice or multiyear ice with first year ice as a result of current changes or unusual wind conditions. Both these types of ice, due in the first case to low salinity, and

in the second case to high amounts of consolidation, represent increased hazards to offshore structures (Cammaert and Muggeridge, 1988).

2.1.4 Properties and Materials Testing Procedures

Ice testing, like its soil mechanics equivalent, attempts to characterize the mechanical properties of the material in question. In the case of ice, as in some soils, strength is anisotropic due to its crystalline structure. Material testing of ice is done in flexure and in compression. Mellor (1983) states that the mechanical properties of ice are complex due to the high homologous temperature it exists at in nature. Homologous temperature is the dimensionless ratio of the ambient temperature to the melting temperature of a substance. Sinha (1984) discusses the influence of strain rate, temperature, and stress state on mechanical properties.

2.1.4.1 Testing of Ice beams

In an effort to standardize the types of testing done on ice, IAHR has published a number of papers on methods of testing, including Shwarz *et al.*'s (1981) recommendations for the measurement of the mechanical properties of ice. Measurements of the flexural strength of ice form important inputs for many ice load models which assume ice fails in flexure against inclined structures.

Three types of beams are commonly tested in flexure: cantilever, 3 point loading simply supported, and 4 point loading simply supported. Their response is analysed assuming linear elastic material behaviour, which is a simplification of the complex stresses

encountered in the field. This is recognized and a series of recommendations to minimize these effects are included with the IAHR standards. The geometry of the beam is recommended to be a length 7-10 times the ice thickness and a width 1-2 times the ice thickness. These recommendations are in place to attempt to isolate flexural failure mechanisms from shear failure mechanisms, as a short beam may fail by a combination of these two modes. Stress relief in the form of radii cut at the roots of cantilever beams, especially in freshwater ice, are required to give meaningful results. Loading rate also affects the results. Määttänen's (1975) rule for loading rate is to choose a rate corresponding to failure after approximately 1 second. Other possible factors affecting measurements include loading direction (related to what these data will be used for), instrumentation (number of load and deflection measurements and sampling rate), test conditions (properties of the ice such as air bubbles, structure, etc., and of the test site such as snow cover, and air temperature), beam preparation, statistics (to optimize the number and type of measurements) and brine volume (Schwarz *et al*, 1981).

2.1.4.2 Flexural Strength of Ice

Timco and O'Brien (1994) report on a relationship between flexural strength, σ_f , and brine volume, v_b .

$$\sigma_f = 1.76e^{-0.588*\sqrt{v_b}}$$

and gives a correlation coefficient (r^2) of 0.77. The model is further validated by the fact that σ_f for $v_b=0$ is 1.76 MPa, which is close to the average flexural strength of freshwater ice of 1.73 MPa reported by Timco and O'Brien (1994). A survey of over two thousand

four hundred flexural measurements was conducted, and flexural strength values reported range from 0.3 MPa to 3.0 MPa for freshwater ice, and from 0.1 MPa to 1.5 MPa for sea ice (Timco and O'Brien, 1994). Flexural strength testing causes non-uniform stress distributions in ice and requires the researcher to make a variety of assumptions about the material behaviour of ice to interpret the results. For this reason, flexural strength is regarded as an index for other ice properties, as opposed to being a material property itself (Timco and O'Brien, 1994).

2.1.4.3 Compressive Strength of Ice

Timco and Frederking (1990) developed a relationship for the compressive strength of ice sheets based on the comparison of small scale measurements to large scale field program measurements. The advantage of this method is that it requires only simple input parameters – air temperature, ice thickness, and bulk density – which are incorporated into an expression for the total porosity of ice. The porosity value serves as an input to one of three equations (chosen based on the orientation of the axis of loading with respect to the internal structure of the ice). Parametric variation was used to check the effects of each type of measurement on model outputs for a variety of strain rates. When the model predictions of ice sheet strength were compared to large scale test results, there was 'excellent agreement' between the two scales (Timco and Frederking, 1990).

2.1.4.4 Flexural Strength Compared to Compressive Strength of Ice

According to Figure 10 of Timco and O'Brien (1994), the ratio of compressive to flexural strength based on the two preceding references is in the range of 6.5 to 8 for an Arctic

structure based on strain rates on the order of $5 \times 10^{-4} \text{ s}^{-1}$. This is the basis for the choice of structures with inclined slopes at the waterline, which are designed to promote failure of ice in flexure, theoretically reducing the ice load on the structure and increasing icebreaking efficiency.

2.1.5 Rubble Pile Definition

Before proceeding further, it is necessary to define precisely what is meant by an ice rubble pile for the purposes of this study. A rubble pile is defined as an accumulation of pieces of ice that have been derived either directly from ice-structure interaction, or from the processes directly subsequent to ice-structure interaction (i.e. ice falling from the top of an ice-structure interaction interface, etc.). In addition, the accumulation height must be significant - i.e. two ice thicknesses or more in addition to the parent level ice sheet or floe (which is commonly in direct contact with the structure). The height of the rubble pile is measured from the top of the level ice sheet, and extends to the location of maximum height of distinct fragments of rubble. It is important to note that the top of the level ice may not always be at the waterline in the case of a conical structure. Observations have been made in both the centrifuge and large testing basins of cases where the ice sheet in the vicinity of a conical structure is inclined with respect to the water surface. For simplicity, ice rubble pieces are commonly depicted as rectangular in shape in order to make clear that they are the product of the parent level ice sheet. In both the prototype and centrifuge, this simplistic depiction does not match observations (Pfister *et al.* 2002). Piece size is often well graded (varies from small pieces on the scale

of a few grains of ice to large chunks) and irregular in shape. See Figure 2. 1 for an illustration of these definitions.

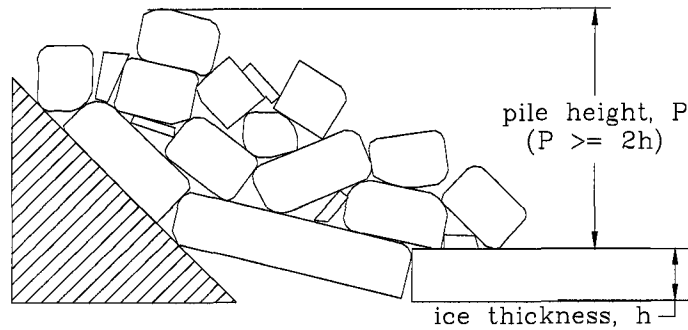


Figure 2. 1: Rubble pile dimensions.
Incoming level ice and an associated rubble accumulation.
A rubble pile has a height (P) greater than or equal to
2 times the level ice thickness (h).

Important parameters governing the strength of ice rubble are the topic of current research. Because of its particulate nature and the way rubble clears around most offshore structures, measures of flexural and compressive strength of intact ice are not the optimum measures to define ice rubble. Both the unconsolidated and consolidated cases are of interest for investigation of ice ridges. McKenna *et al.* (1996) investigated the *in situ* shear strength of model ice rubble ridges using a punch technique. The experiment consisted of vertical displacement of a steel platen through ice ridges constructed from model ice. Different rates and platen diameters were tested. Analysis of the results was conducted using the Meyerhof and Adams technique for pullout of a shallow circular footing (McKenna *et al.*, 1996). The objective of this analysis was to

establish the parameters of the Mohr-Coulomb failure envelope for ice rubble, tangent angle ϕ and cohesion c . The results showed that, as expected, consolidated ridges were more resistant to shear than unconsolidated ones (McKenna *et al.*, 1996). For the unconsolidated case, parameters ϕ and c were estimated at 36° and 0.44 kPa respectively; however, no statistically significant results were obtained for the consolidated case (McKenna *et al.*, 1996). The method was deemed impractical for use in field tests because hundreds if not thousands of data points would be required.

2.1.6 Force Models for Ice Loads on Structures

All ice force models are developed by making a series of assumptions regarding interaction geometry and ice failure processes. The processes can be divided into two categories: initial formation of ice rubble, and the steady state condition of a sustained rubble piling event. None of the models reviewed in the literature address the possibility that an ice rubble pile may not form during the interaction of level ice with upward breaking conical structures.

Two of the most commonly cited models are those of Croasdale (1994) and Nevel (1992). Croasdale's (1994) model was originally developed for use in two dimensional (2-D) interactions and has been subsequently adapted for use in three dimensions (3-D). It has been used because of its computational simplicity in probabilistic analyses. Nevel's (1992) more complex model relies on computer code to perform detailed calculations of each component of load. It contains an arguably more sophisticated

treatment of the ice sheet's geometry. The Croasdale model has been found to give results comparable to the Nevel model (Croasdale *et al.*, 1994).

2.1.6.1 Croasdale's Ice Force Model

Croasdale's original analytical 2-D model of an elastic beam on an elastic foundation was developed in the late 1970s. In 1980, the model was modified for 3-D effects. In its most basic 2-D form, the model sums the total horizontal force experienced by the structure from two components: the bending failure load of the ice beam, and the load required to push ice pieces up the face of the structure (Croasdale, 1994). Modifications introduced to expand the model's scope to 3-D include increasing the width, D , of the failure area by the ratio of the characteristic length, l_c , to structure width. For circumstances where D is large compared to l_c , the 2-D and 3-D values converge. Modifications were also made on the basis of in-plane compressive forces causing an apparent increase in the flexural strength of the ice sheet; on the basis of requiring additional horizontal force to overturn ice pieces at the top of the slope; and on the basis of the presence of ice rubble pieces on top of the ice sheet.

Croasdale (1994) describes the process of ice rubble pile initiation on an inclined plane or conical structure and steady state rubble interactions as follows:

“(1) initially ice fails and rides up (as represented by the existing equations), (2) the ride-up continues a small distance up the vertical shaft before ice blocks fall back onto the advancing ice sheet, (3) a rubble pile forms in front of the structure, initially supported by the advancing ice sheet, (4) for a while the advancing ice continues to be pushed through the rubble surcharge to fail against the slope of the structure, but the rubble surcharge

eventually breaks the advancing ice sheet due to its weight. The sequence is then repeated; or for a very wide structure the rubble doesn't clear and the advancing ice fails against the ice rubble in a random rubble building process.”

Based on this description, the changes made to the model for the presence of ice rubble were: the addition of a force component required to push the level ice sheet through the ice rubble, the addition of a force component required to push the pieces of ice up the slope through the ice rubble, and the addition of the force required to lift and shear the ice rubble on top of the ice sheet. The resultant model has a total of five forces contributing to the total horizontal force – the first two components from the 2-D model modified for 3-D and the three subsequent forces caused by the presence of the ice rubble. It is implied that all level ice sheets interacting with conical or sloping structures will go through the rubble building process as described by Croasdale, and that the ice sheet fails in flexure throughout the interaction and rubble accumulation sequence.

2.1.6.2 Nevel's Ice Force Model

Nevel's model (1992) is developed in a highly mathematical and theoretical fashion. An infinite ice sheet is assumed to come in contact with a conical structure with a vertical neck and break into a series of truncated wedges. As the ice sheet comes in contact with the cone, radial cracks form. The ice rides up, and after a critical distance, circumferential cracks form at the base of each wedge (either simultaneously or sequentially). Maximum stress is assumed to occur when the center wedge fails. The wedges are assumed to entirely cover only the front half of the cone. Increased force is required to break subsequent wedges due to the friction and self weight of the above

pieces. Nevel (1992) assumes no shear forces are transmitted between wedges – all stresses are in the plane of the ice sheet.

Force components are primarily normal forces (caused by self weight of the ice) and frictional forces (resisting motion of the ice up the cone). Nevel also defines active and passive ice forces in relation to the position of an ice piece relative to the change in slope of the cone from inclined to vertical. Active ice forces are caused by ice jamming against a change in slope and are equal to the forces required to cause an ice wedge to overturn. Passive ice forces are the self weight and friction from a given ice piece, plus any extra forces from pieces of ice above it (Nevel, 1992). As in Croasdale, the ice sheet is assumed to rest on an elastic foundation, and the breaking of the ice sheet into pieces is based on the equation for a simply supported beam under its own weight. Nevel does not introduce effects from ice rubble, nor mention the possibility of ice rubble accumulation on the advancing level ice sheet. Flexural failure of wedges is the underlying basis of this analysis.

2.1.6.3 Shear Failure of Level Ice

Lau *et al.* (1999) introduce the possibility of ice failing in shear against a conical structure. The authors examine a variety of data from conical structures, an inclined plane, and a series of icebreaker hulls. Based on the geometry of the cracks around the structures and the size of the resulting ice pieces, the dominant failure modes were determined. A parametric analysis of important variables including ice strength and thickness was conducted, and equations developed to predict the size of ice pieces. The

authors note that the pattern of broken ice observed was different from that predicted by simple elastic theory, especially for thicker ice. Shear failure across the ice thickness is proposed as an explanation for this difference. An equation for the expected size of pieces from an ice-structure interaction is developed in terms of characteristic length, and predicts piece size on the order of 0.1 to 0.2 times the characteristic length of the parent ice sheet (Lau *et al.*, 1999).

2.1.7 Previous Rubble Pile Observations

Hoikkanen (1985) reported some of the first full-scale rubble observations, gathered at the Kemi-I lighthouse located in the northern Gulf of Bothnia. The interactions were mainly with level ice 5 to 70 cm thick; some instances of rafted ice and pressure ridges were also observed. The Kemi-I geometry bears remarkable similarity to that of the Confederation Bridge. The structure is concrete encased in steel; the slope is 55° from the horizontal; and the waterline diameter is 10 m. Water depth at the structure is 12 m, and the ice is first year saline. Ice velocities in the region range from nearly 0 m/s to upwards of 0.2 m/s with no prevailing direction. Direction of ice movement can change slowly or suddenly, and wind and sea currents are the predominant driving forces (Hoikkanen, 1985).

For thin ice (5-20 cm) breaking against the cone, floating rubble piles were observed, and failing ice “started to pile up until the rubble reached a stable quantity” (Hoikkanen, 1985). For thicker ice (30-70 cm) several ice breaking and clearing patterns were

observed. For slow interactions (velocities on the order of meters per hour), the ice behaved in a ductile fashion, with the appearance of relatively large, coherent segments peeling away from the structure. For increased speeds, ice rubble tended to form in front of the cone both above and below the level ice sheet. A transition between different failure modes was remarked on: “when the rubble had grown sufficiently, the ice failure mode was by crushing” (Hoikkanen, 1985). The ice pieces resulting from this type of interaction were small and irregular in shape (compared with the diameter of the structure). Hoikkanen also remarked that the level ice sheet was fed through the rubble pile and failed against the structure itself. This observation is attributed to the confining effect of ice rubble above and below the waterline.

Izumiyama *et al.* (1994) adapted a formulation for ice-structure interactions formerly used to predict piece size in the wake of a passing ship . The test series involved level ice interacting with faceted upward breaking cones. Ice rubble accumulations in front of upward breaking faceted cones are categorized into four types:

- Type A – pieces of parent ice sheet on front facet of cone
- Type B – single thickness of pieces on top of broken parent ice sheet, mostly supplied by overturning at the neck of the cone
- Type C – as in B, except the pieces break as they cascade down the front of the cone
- Type D – apparently random formation of a large number of randomly shaped and oriented ice pieces, relatively large piece size.

D-type rubble accumulations are the most important observations made, as they coincide with the largest increase in ice force on the structure. Facet orientation and structure geometry strongly influence the probability of rubble pile formation in this test series. This follows as with an 'edge on' orientation (angular discontinuity in cone face parallel to direction of ice travel) of a faceted cone dictates that there will be a very small area available for rubble accumulation. For this reason, the patterns described in Izumiyama *et al.* are not seen in the tests studied in this thesis because the structures of interest were smooth cones, which do not have the same distinct geometric characteristics as faceted cones.

2.2 PROTOTYPE CONDITIONS – THE CONFEDERATION BRIDGE

The Northumberland Strait is part of the Gulf of the St. Lawrence, located on the east coast of Canada. A summary of historical data regarding ice conditions is outlined in the environmental study for the bridge, conducted by Bercha *et al.* (1987). Ice conditions in the Strait can be characterized by dynamic pack (level) ice conditions and the presence of both consolidated and unconsolidated first year pressure ridges. Grounded ice rubble occurs along the shoreline, and grounded shear ridges have also been observed. Ice features which include one or more of the aforementioned categories have also been observed (Williams, 1996). All ice features are first year, and icebergs are not encountered due to shallow water and latitude (Brown *et al.*, 1998). This thesis is focused on the level ice condition. The mean thickness of level ice in the Strait was measured to be 0.64 m (Williams, 1996). The mean drift speed of level ice in the Strait

was measured to be 0.23 m/s (Williams, 1996). Table 2.1 outlines some of the other physical properties measured during this test program.

Table 3. 1:Ice Properties in the Northumberland Strait.
Seasonal variation in the material properties of ice are noted.

	Winter	Spring	Units
Mass density of water, ρ_w	1.024	1.024	Mg/m ³
Flexural strength of ice, σ_f	450	300	kPa
Young's Modulus of ice, E	3.5	0.5	GPa

(after Williams, 1996)

Water in the Northumberland Strait is slightly saline. The piers of the Confederation Bridge are tapered cones at an angle of 52° from the horizontal at the waterline and have an average waterline diameter of 14.1 m (Brown *et al.*, 1998). Approximately 2.5 m above the waterline, the diameter is 10.2 m and the slope of the cones increases to 78° from the horizontal.

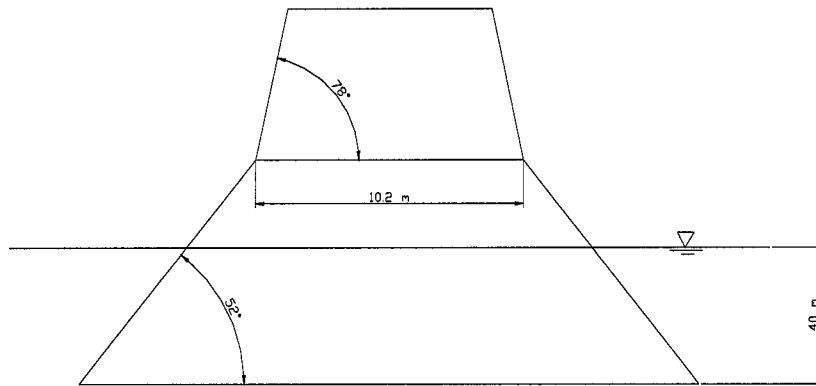


Figure 2. 2: Confederation Bridge pier geometry (after Brown *et al.*, 1998).

Several of the bridge piers have been instrumented with inclinometers and pressure panels to measure ice forces. These data that are being gathered by this monitoring program are subject to a confidentiality agreement; however, Mayne and Brown (2000) have released a paper outlining some preliminary results. This is currently the only source for rubble pile heights and associated ice thicknesses in the prototype case available in the public domain. Ice thicknesses range from 0.3 m to 1.5 m, velocities range up to 1.5 m/s, and pile heights range from 0.5 m to 7.5 m.

2.2.1 Ice Rubble Accumulation at the Confederation Bridge

Observations collected during the Confederation Bridge Monitoring Program include inclinometers to indirectly measure global ice loads, ice force panels for direct measurement of local ice pressure, and video records detailing ice conditions and kinematics (Brown *et al.*, 1998). An ‘event’ is defined as an accumulation of ice rubble,

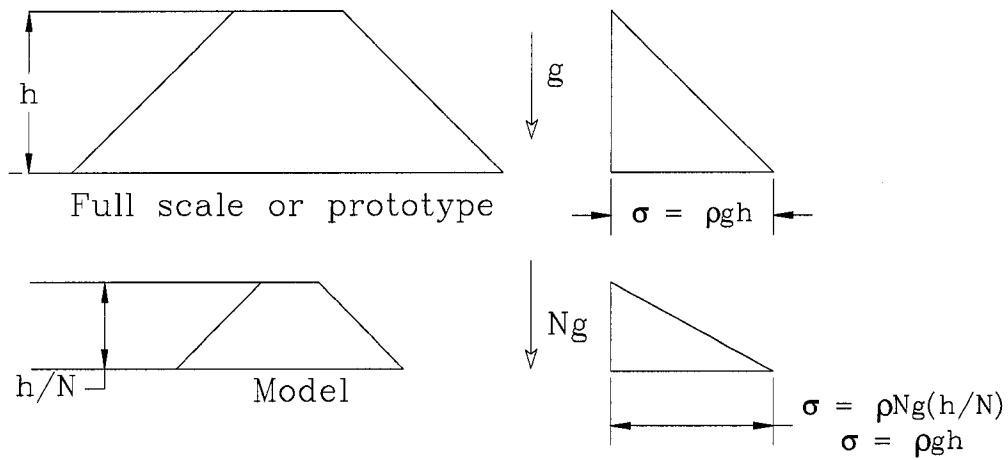
illustrated in Figure 2. 1. Croasdale *et al.* (2003) detail an extensive field program designed to measure the shear strength of first year ice rubble. Mayne and Brown (2000) indirectly address the issue of the incidence of rubble pile formation by acknowledging that a non-event is possible: “For a rubble pile to form, the advancing ice sheet must be failing in a manner that will support a rubble pile, such as upward bending or crushing. When the failure mode changes to floe splitting or a plug failure, the pile will collapse or submerge and be cleared”. This paper fails to comment on the comparative frequency of ice-structure interactions which do or do not result in ice rubble accumulation. The strength of ice rubble has been measured in the Northumberland Strait in a series of field programs, see Croasdale *et al.* (2003).

When ice rubble does form, the first pieces to be produced following flexural failure of the ice sheet are large compared to those that are formed when the rubble pile becomes significant and approaches a steady state condition. The surface condition of the floe influences the angle of repose of the rubble pile. The pile is steeper if the parent ice sheet is snow covered, which implies a greater friction coefficient (Mayne and Brown, 2000). Rubble piles are generally observed to have their maximum height and depth (distance from edge of structure to edge of rubble accumulation) parallel to the direction of ice travel, and their minimum in the clearing planes perpendicular to the direction of ice travel (Lau, 1999). The clearing of ice rubble piles is commonly associated with the downward flexural failure of the approaching ice sheet (Mayne and Brown, 2000).

Two variables commonly thought to influence the height of a given rubble pile are ice thickness and ice velocity. Mayne and Brown (2000) described the relationship between the influence of ice thickness and floe velocity on the height of the rubble pile. Their data suggest an inverse relationship between pile height and velocity, described by a second order polynomial. Rubble pile height and thickness appear to be related, and two different fits to these data were proposed: a second order polynomial and a power relation. In both cases the potential relationships are fit to the extreme values, but it is noted that average rubble pile events have heights approximately half the maximum observed values, typically about 3 m.

2.3 CENTRIFUGE MODELLING

Centrifuge modelling has been used in soil mechanics modeling and in a wide variety of other gravity dependent problems (Schofield, 1980). By decreasing the size of a structure and increasing the gravitational acceleration experienced by this smaller model, stress conditions resulting from body forces in the prototype are reproduced. This relationship is illustrated in Figure 2. 3, showing the example of an earth embankment. This technique has been proven effective in several applications and is an inexpensive alternative to full scale testing (Lau *et al.*, 2002, Taylor, 1995).



Stress at corresponding points is similar

Figure 2. 3: Principles of centrifuge modeling.
 Prototype and model stress distributions for centrifuge
 and 1 g models (after Schofield, 1980).

Previous work in the area of centrifuge modeling of ice-structure interaction includes that of Clough and Vinson (1986), Lovell and Schofield (1986), and Phillips *et al.* (1994). The test program at C-CORE, funded by a joint NSERC/NRC Research Partnership grant, included a test series in the ice tank at IMD. The purpose of the project was to compare ice loads and failure mechanisms under different modelling conditions, i.e., a comparison between results in a geotechnical centrifuge and an ice tank. Lau *et al.* (2002) summarize the results of the force comparisons. This study details the findings of this test series in the area of ice failure processes and ice rubble accumulation patterns.

C-CORE's geotechnical centrifuge is an Acutronic 680-2 (Phillips *et al.* 1994) with a radius of 5.5 m to the platform in the articulated position, and can accommodate experimental packages 1.1 m × 1.4 m in plan and up to 1.2 m in height over the entire platform and up to 2.1 m in height in the centre of the platform. The maximum rotational rate of the centrifuge is 189 rpm, which corresponds to an acceleration of 200 gravities at 5 m radius (Lau *et al.*, 2002). Tests were conducted at 1:30, 1:60, 1:90, and 1:120 geometric scales. The model upward breaking conical structure had a 45° slope and a waterline diameter of 120 mm. Ice thicknesses varied from 5 mm to 17 mm. Applying the appropriate geometric scale factor, this corresponds to a structure 3.6 m, 7.2 m, 11.0 m, or 14.8 m in diameter at the waterline respectively, and ice thicknesses between 0.6 m and 2.0 m in prototype. Flexural strength of ice is found to be independent of inertial acceleration. Early ice load data were 'in reasonable agreement with the loads predicted by various theoretical and semi-empirical algorithms' (Barrette *et al.* 2000). There are some limitations of scaling ice-structure interaction in the centrifuge. The thickness of the ice sheet is small in relation to the thickness of the seed layer when compared with field conditions (Barrette *et al.* 2000). Lau *et al.* (2002) detail the reduction in salinity of the water used in this test series to temper the strength of saline ice used in the centrifuge.

The physical properties of both freshwater and saline ice sheets grown at high inertial accelerations were examined by Barrette *et al.* (1998). Using C-CORE's 840×1075 mm cold box, ice was grown at 30 gravities (*g*) followed by ice-structure interaction testing at

up to 120 g. During the interaction phase, the model pier (mounted on rails and connected to the servo drive by a steel aircraft cable) was pulled through the ice sheet as per Figure 2. 4.

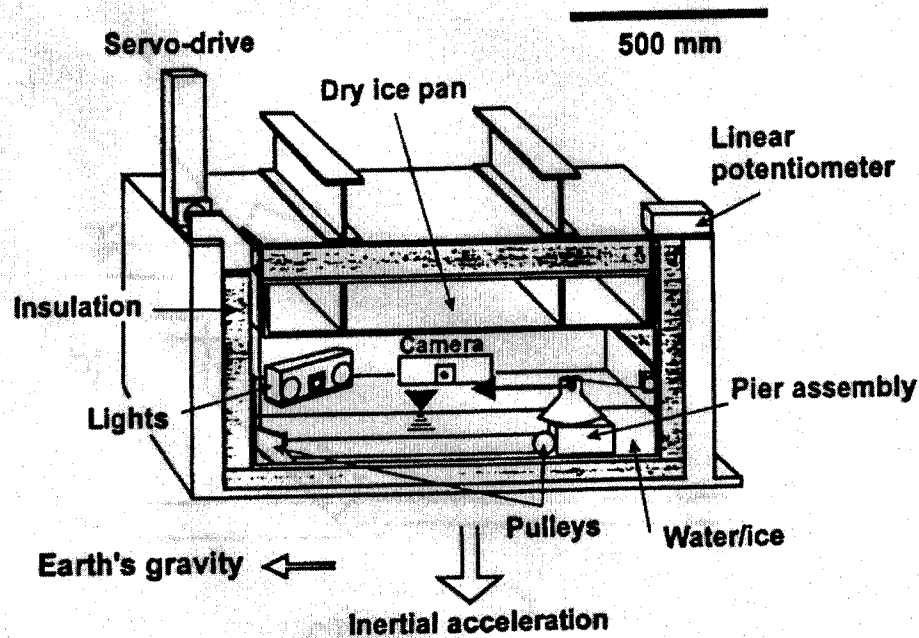


Figure 2. 4: Centrifuge package.
Cold box setup for ice-structure interaction testing
in the C-CORE centrifuge (after Barrette *et al.* 2000).

At the Confederation Bridge, individual floes move past the structure; however, this configuration is not possible in the small space available in centrifuge testing, so the situation was reversed in the cold box with the structure moving through the ice sheet. Tests were monitored using a CCD camera mounted within the package (Barrette *et al.*, 2000).

2.4 IMD TEST SERIES

Ice tank testing represents the current industry standard for ice-structure interaction modelling. The facility at IMD is one of the largest in the world. The ice tank is $12\text{ m} \times 90\text{ m}$ in plan with a usable ice surface of up to $12\text{ m} \times 76\text{ m}$, and in this configuration, the structure is translated through the ice sheet. The ice formulation is NRC EG/AD/S CD (ethylene glycol/aliphatic detergent/sugar corrected density), with a flexural strength range of 10 kPa to 120 kPa, and a thickness range of 10 mm to 150 mm. Typical values for ice properties from the level ice test series conducted by Lau *et al.* (2000) of interest in the test series discussed in this thesis are outlined below.

Table 2. 2: EG/AD/S CD Ice Properties

	Maximum	Minimum	Units
Young's modulus, E	226900	41700	kPa
Flexural strength, σ_f	44.1	16.8	kPa
Mass density of ice, ρ_i	887	855	kg m^{-3}
Ice thickness, h	117	34	mm

After Lau *et al.*, 2000.

The model used in this test series was an upward breaking smooth conical structure with a waterline dimension of approximately 1 m and a slope of 45° . This represents a 1:12 scale with the prototype case of interest. Tests were also conducted with a 60° cone with a waterline diameter of approximately 1.2 m. The model was instrumented with an array of load cells and mounted on the towing carriage in the ice tank at IMD. Six different ice sheets were grown and tested in this series, with the objective of encompassing a variety of ice thicknesses and interaction velocities. Ice forces exerted by the level ice sheet on

the cone were recorded over time, and video recordings were made of the interaction processes.

McKenna and Spencer (1994) conducted a similar series of tests at the same facility using a 60° smooth cone. Prototype ice thicknesses ranged from 0.5 m to 1.5 m; prototype waterline diameters were 11.3 m and 14.8 m. Interactions occurred at velocities between 0.1 m/s and 1.5 m/s; the majority of tests were run at 0.5 m/s. As in Lau *et al.*'s (2000) tests, the ice sheet cracked radially and circumferentially as it passed the cone but rubble (as defined in this thesis) did not accumulate on the cone. "These pieces rode up the entire front half of the cone and cleared around the sides except for the occasional block which fell back in front. In all cases, there was no significant accumulation of rubble on top of the ice." (McKenna and Spencer, 1994). Even when the cone was purposely moved through rubble in the preliminary portion of an interaction, a rubble pile was not sustained into steady state indentation (McKenna and Spencer, 1994).

2.5 FRICTION AND ICE-STRUCTURE INTERACTION

An examination of the theory of friction between solid surfaces was investigated in the context of prediction of ice rubble accumulations. Knowledge of the friction coefficient between ice and the surface of a structure, as well as the friction coefficient between pieces of ice, may be instructive when investigating ice rubble. A summary of the material presented by Mitchell (1993) on the theoretical basis of friction follows.

The two basic laws of friction first proposed by Da Vinci in 1500 and then Amonton in 1699 are as follows: frictional force is proportional to the normal force; and frictional resistance between 2 bodies is independent of the size of the bodies. True friction, defined as resistance to sliding along particle surfaces, accounts for half or more of the peak strength and most of the residual strength of soil. The true friction coefficient, μ , is given by the following relationship: T is the force exerted on the object to initiate motion and N is the force normal to the object in motion. The true intergrain friction angle, ϕ , is a function of the mineral composition of soil. Mostly constant over a range of surface roughnesses, μ does not go to zero as surfaces become smooth.

$$\mu = \frac{T}{N} = \tan \phi \quad (2.2)$$

Static friction results from cohesive forces between contacting surfaces. Because the actual contact area is very small, the cohesive forces must be very large. Terzaghi (1920, as cited in Mitchell 1993) identified that all solid surfaces (even those which appear smooth) have minute localized “bumps”, which he called asperities, on the scale of 10 to 100 nanometers. Terzaghi defined the actual contact area, A_c , as the normal force (N) divided by the yield strength of the material (σ_y), and postulated that yielding occurred at such contacts. If this is the case, then the maximum shear force (T) which can be resisted by the yielded zone is a product of the contact area (A_c) and the shear strength of the material (τ_m). These two relationships can be combined to show the dependence of μ on shear strength and yield strength:

$$\mu = \frac{T}{N} = \frac{A_c \tau_m}{A_c \sigma_y} = \frac{\tau_m}{\sigma_y} \quad (2.3)$$

This theory was further developed in the 1950s and 1960s, and is commonly referred to as the adhesion theory of friction. The two ideas central to this theory are surface roughness and surface adsorption. Surface roughness describes the asperities on a given surface. The slopes of asperities are typically very shallow and range from 120 to 175 degrees between two lines tangential to the slopes of a given asperity. The molecular structure and composition of the contacting asperities determine the magnitude of τ_m . Surface adsorption is explained by the kinematic theory of gases, which says that in a short time all surfaces become covered with a film of adsorbed material, unless they are under high pressure. This film acts to further reduce the contact area. According to the adhesion theory of friction, there are two types of junctions. If the asperities in contact yield and undergo plastic deformation, the junction is plastic. If no permanent deformation occurs, the junction is elastic. In the case of ice, the former is more likely to occur than the latter when the ice rubble is in compression, as individual pieces may fail locally under the weight of adjacent pieces. This may result in the development of apparent cohesion in the rubble mass. It is less likely that a soil would be subjected to loads which would exceed the yield stress of the grains, which makes the possibility of a truly cohesionless mass more likely for this material. The time dependency of such contacts must also be investigated.

The Canadian Hydraulics Centre recently released a detailed report on the friction of sea ice on construction materials (Frederking and Barker, 2001). The tests investigated the change in friction coefficient corresponding to changes in the material surface, surface

characteristics such as wetness, normal pressure, temperature, and speed of interaction. The tests were conducted by a mobile carriage with a block of saline ice affixed to it, which traversed a strip which contained samples of the various surface materials, including wood, smooth concrete, rough concrete, steel, and corroded steel. Measurements of normal and tangential forces between the ice sample and surface were obtained. The ice-structure friction coefficient was found to depend slightly on temperature (higher temperatures correspond to slightly higher coefficients); a similarly slight dependence appeared to exist for confining pressure (higher pressures correspond to slightly lower coefficients). For velocities above 5 cm/s, the average value of the sea ice friction coefficient for interactions with smooth concrete or painted steel was 0.05 and increased to 0.10 at slower speeds of 1 cm/s. For rough concrete and corroded steel, the average value of the sea ice friction coefficient was 0.10 for speeds greater than 10 cm/s and increased to 0.20 at speeds of 1 cm/s (Frederking and Barker, 2001). These results are highly applicable to the prototype case as the majority of piers of the Confederation Bridge are concrete. Enoki *et al.* (1990) also conducted friction coefficient research for freshwater ice-steel interfaces under high pressure. As in the CHC report, the friction coefficient decreased with increasing pressure; however, the friction coefficient increased with decreasing in temperature. The values of μ reported range from 0.02 to 0.13, and though they are reported in terms of static and kinetic, velocity is not specifically mentioned as a parameter of interest in this study. Friction coefficient values are reported by Barrette *et al* (1999) for the centrifuge models as 0.13 \pm 20%, i.e. 0.10 to 0.16. Lau *et al* (1988) reports a value of 0.15 for the models used in the IMD test series.

Gershunov (1987) presents a treatment of friction between a conical structure and an unconsolidated or poorly consolidated rubble field. Assuming a unidirectional interaction between a rubble field of homogeneous mechanical properties and an upward breaking conical structure, an algebraic expression is developed using polar coordinates and force balance to determine if initiation of an ice rubble piling event is possible. The results show that for a given angle from the horizontal, α , there is a minimum friction coefficient, μ , which must be exceeded for formation of an ice accumulation zone.

Table 3. 2: Minimum friction coefficients for ice rubble accumulation

α	15°	30°	45°	60°	75°	90°
μ	3.73	1.73	1.00	0.58	0.26	0

after Gershunov (1987)

According to this method, a rubble pile would be predicted for all vertical structures (friction coefficients cannot be zero) and not predicted for any structure with a slope less than 45° (as friction coefficients should not exceed 1.0). Field observations (Mayne and Brown, 2000, Pfister *et al.*, 2002) show that these are unrealistic boundary conditions, and studies of friction coefficients indicate that if this were a complete model then rubble piles should never occur. This model assumes that there are no pieces of ice above the piece of rubble riding up in the force balance, and no energy is required to deform the ice field as it already consists of rubble. This approach may be used in part to explain the initiation of ice rubble accumulation: when the forces moving a block of ice up the slope of a structure are exceeded by the frictional resistance to that motion, the piece ‘sticks’ in place and acts as a nucleation point for ice rubble accumulation.

2.6 FRACTURE MECHANICS AND ICE-STRUCTURE INTERACTION

Fracture mechanics is proposed as a method of predicting peak load on a structure, based on the premise that peak loads will occur at the transition from creep to brittle failure (Hallam, 1986). Bhat *et al.* (1991) propose a scheme to examine failure by these two mechanisms, and developed equations for both global and local failure. The ice floe is approximated as an elastic-brittle disc, colliding with a rigid bottom founded vertical cylindrical structure. The structure penetrated the floe until the floe either a) has decelerated and stopped the interaction, or b) failed by global processes (splitting) or local processes (rubbling) and subsequently cleared around the structure.

Two model configurations were considered by Bhat *et al.* The first (model A) assumed no penetration of the structure into the floe, with a small rectangular contact area between the floe and the structure. Model B assumed a semi-circular notch had formed and that the load was uniformly distributed on the structure around the notch. The stress state was determined along the axis perpendicular to the direction of travel of the floe using finite element analysis. The floe was treated like a specimen in a Brazil rock mechanics test in a state of uniaxial tensile loading. The material was assumed to follow the Drucker-Praeger failure criterion. Model B is considered to be most relevant for the ice-structure interaction problem as penetration of the conical structures into the ice floes was commonly observed in the prototype case.

Integrating around a semi-circular notch and applying these findings to the Drucker-Praeger failure criterion, agreement was found between the analytical solution and that proposed by Bhat *et al.* (assuming a valid finite element computation). For purposes of comparison with Bhat, it is assumed that flexural strength (σ_f) is equivalent to tensile strength (σ_t). The force required to initiate ice rubble accumulation is

$$P_i = 2.06 \times \sigma_f \times h \times r \quad (2.4)$$

where σ_f is the flexural strength of ice, h was the ice thickness, and r is the structure radius. For splitting or global failure, the force required is

$$P_s = 0.62 \times K_{IC} \times \sqrt{2R} \quad (2.5)$$

where K_{IC} is the fracture toughness and R is the floe radius. For a given interaction event, the failure mode requiring a lower force to initiate is more likely to occur.

Palmer (1991) integrates the considerations of centrifuge modelling with fracture mechanics. (Upper case letters denote prototype quantities and lower case letters denote model quantities.) As per section 2.3, he develops the following equation for classical centrifuge modeling:

$$\frac{S}{s} = \frac{G}{g} \times \frac{D}{d} \times \frac{L}{l} \quad (2.6)$$

where s is stress, g is g level, d is density, and l is length. The scaling factor is equal to G/g , (the number of gravities experienced by the model in the centrifuge divided by acceleration due to gravity). Therefore, for a geometrically similar model, stresses are preserved, and g level (n) is inversely proportional to model size ($1/n$). The same

principle is then applied for a brittle material (such as ice) where failure is governed by the stress intensity required to form cracks. Palmer shows that crack length, c , does not scale as a material property but rather as a function of geometry. For example, in a simply supported beam, the minimum size of a crack on the tension side of the beam will not decrease by 100× simply because the beam size decreases by 100×. For a material where stress intensity is related to stress by $K_{IC} = \text{constant} \times \text{stress} \times (\pi \times \text{crack length}, c)^{1/2}$, if stresses model, then

$$\frac{K_{IC}}{k_{IC}} = \frac{G}{g} \times \frac{D}{d} \times \frac{L}{l} \times \left(\frac{C}{c} \right)^{1/2} \quad (2.7)$$

assuming that the density of the model material is the same as the prototype. In this case, then

$$\frac{g}{G} = \frac{L}{l} \times \left(\frac{C}{c} \right)^{1/2} = \left(\frac{L}{l} \right)^{3/2} \quad (2.8)$$

which shows that to scale fracture, crack length should be considered relative to the structure size. This scaling is inherent in Bhat *et al.*'s analysis when determining if a floe will split – if the crack formed is a critical length (percentage of floe diameter), then it will propagate and the floe will split.

2.7 DIMENSIONAL ANALYSIS

Dimensional analysis is a powerful tool that allows reduction of the number of parameters of interest in a given problem by combining variables into dimensionless

groups. This technique is particularly useful in problems where the number of variables is high and the system is too complex for effective treatment by a rigorous mathematical model (Sharp and Moore, 1983). Several methods of partial analysis are available; however, for use in engineering (particularly experimental work), the most common method is based on Fourier's principle of dimensional homogeneity. This principle is applied each time one conducts a 'units check' when using an equation – any correct equation must have the same units in each term (Sharp, 1981). Critical to the successful use of this dimensional analysis is identification of all the important variables influencing the problem. Following either the Buckingham (Sharp, 1981) or Rayleigh (Sharp, 1981) method, the variable of interest is expressed as a function of the other identified variables which are then presented in 'base unit' form – mass, length, time, etc. For complex problems, an efficient method of reduction of a set of variables into a series of dimensionless parameters is the matrix method, introduced by Sharp and Moore (1983).

Arunachalam (1996) used the matrix method to study the problem of ice-structure interactions in terms of ice pressure and failure mode analysis. A long list of independent variables is identified, including several material properties of ice, geometric aspects of the interaction, velocity, and acceleration due to gravity. The influence of velocity on the behaviour of ice in contact with structure is discussed at some length. Arunachalam (1996) proposes a relationship between dimensionless pressure, $p_e/\rho_i V^2$, and dimensionless strain-rate, V^2/gl_c . A wide variety of data from several test programs was plotted on a log-log chart over a wide range of values of these parameters. However,

both of these parameters are normalized by the same parameter (velocity), and velocity exhibits the widest variation of any of the variables studied. Gravity, g , is constant - all test data included were collected at 1 g . Characteristic length, l_c , will vary somewhat with ice type - saline vs. freshwater etc. but not over a wide range. Ice pressure will vary slightly. Ice density, ρ_i , is relatively constant. Interaction velocity, V , however, can easily vary over 3 orders of magnitude (from mm/s to m/s) and even more widely. As a consequence, it is possible that the apparent relationship between these dimensionless parameters is a result of the presence of velocity on both axes.

Lau *et al.* (2000) discuss the influence of velocity on ice-structure interaction. Two different cone geometries were tested (45° and 60°) at a wide range of velocities (0.005 m/s to 0.5 m/s) in level ice sheets 35 mm to 110 mm thick. The tests were performed in the IMD ice tank. The authors discuss a transition between flexural failure and shear or crushing failure modes. This transition was seen in observations of the ice sheet during interaction with the cone and is supported by data showing increased mean peak force. In the case of the 45° cone, failure was typically by flexure as previous model tests suggest, but showed an increase in mean peak force at velocities above 0.25 m/s. The 60° cone showed a more abrupt change in failure mode at high velocities in thick ice sheets. The shear failure mode was particularly observed at $V=0.15$ m/s for the 117 mm ice sheet tested. The piece size for this failure mode was small, typically less than $15 \times 10 \text{ mm}^2$ and columnar in shape (Lau *et al.* 2000). At the point where these pieces were observed, the authors noted that the pieces formed before any circumferential

cracks were visible. Despite the large quantity of small pieces formed, the rubble accumulation was not significant – a spray of fine chips “cleared around the cone with a small amount of ride up” (Lau *et al.*, 2000). The authors propose a limit of 0.02 for the Froude number (where the Froude number is defined as $V/(gh)^{1/2}$), below which velocity should not affect the failure mode and Froude scaling is unimportant. According to this threshold, given the average conditions at the Confederation Bridge, the Froude number will exceed the critical value of 0.02 (0.09 for an average $h=0.64$ m, and an average $V=0.23$ m/s) implying that a transition from flexural to shear failure may be observed.

3 EXPERIMENTAL METHODS

3.1 CENTRIFUGE DATA

Several test series were conducted in the C-CORE centrifuge to investigate the behaviour of level and rubble ice interactions with structures of varying geometries. This author was intimately involved in the two centrifuge test series which consisted of level ice interaction with upward breaking conical structures. Duties performed included growth and testing of trial ice sheets for use in a database of upward and downward breaking flexural strength, calibration and maintenance of instrumentation including load cells and thermistor arrays, and assisting with package assembly, loading, monitoring, and post test analysis. The rubble accumulations were photographed *in situ* and then collected from the package for storage and subsequent analysis. A schematic of the package, including the arrangement used to pull the model structure through the ice sheet, is given in Figure 2. 4. A photo of typical post-test configuration of the displaced model and resultant altered ice sheets are given in Figure 3. 1 and Figure 3. 2. For purposes of comparison, photos are given of a deformed saline ice sheet, and of a deformed freshwater ice sheet. The differences between the two cases will be discussed in detail later.

Data collected during these tests fell into two phases, as did the testing. The ice growth phase observations consisted of monitoring the temperatures output from an array of closely spaced thermistors, which were used to in combination with an empirical curve to judge ice thickness. Load cell outputs, which would be crucial in the second phase of

testing, were also monitored to ensure quality data could be expected at the time of the interaction phase. Once the ice had reached target thickness, the g-level was increased to test speed. The carriage (with the model structure mounted on it) was then advanced through the ice at a constant rate of 40 mm/s and the output of the load cells and potentiometer were recorded at high frequency to allow construction of force-time and force-displacement curves. Video data was also recorded during the interaction event by a CCD camera. Typical results of interaction events for the saline and freshwater cases are shown in Figure 3. 1 and Figure 3. 2.



Figure 3. 1: Freshwater ice rubble accumulation in the centrifuge. Model structure surrounded by an ice rubble accumulation made up of small pieces following freshwater ice-structure interaction event in the centrifuge.

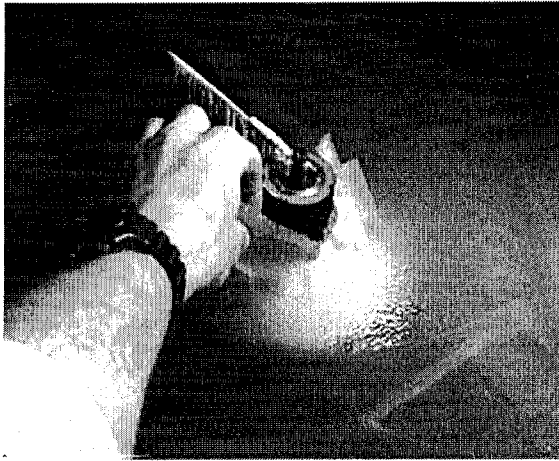


Figure 3. 2: Saline ice sheet deformed following interaction in the centrifuge. Model structure showing typical formation of a series of large ice pieces following saline ice-structure interaction in the centrifuge.

The test series of interest to this research was conducted between September 1999 and January 2000. Nineteen separate tests were run in nine ice sheets of varying thicknesses, salinity, and g levels. The model structure, an upward breaking cone inclined at 45° , had a waterline diameter of 120 mm. The model ice thicknesses ranged from 5 mm to 11 mm. An ice rubble pile was repeatedly observed in freshwater level ice-structure interaction tests in the centrifuge. Because of the model scale, the ice rubble pile and a margin of surrounding level ice had dimensions of less than 0.25 m^2 . Samples of the deformed ice sheet and associated ice rubble accumulation were collected following five different tests. The intact ice rubble cone, which consolidated during centrifuge spindown, was preserved in a chest freezer at approximately -20°C until further analysis was conducted. See Table 3. 3 for a listing of all centrifuge tests completed. Note that tests ICESTR31 to ICESTR 34 were in freshwater ice and tests ICESTR35 to ICESTR39

were in saline ice. See Appendix A for a log of photographs of the cones and section locations.

Table 3. 3: Centrifuge test series summary.

TEST CODE	g-level	Flexural Strength* (kPa)	h (m)	V (m/s)	W/2 or 'r' (m)	E* (kPa)
ICESTR31	30	2300	0.0153	0.04	0.0615	2760000
ICESTR31+	90	2300	0.0158	0.04	0.0615	2760000
ICESTR32	60	2300	0.011	0.04	0.0615	2760000
ICESTR32+	120	2300	0.0115	0.04	0.0615	2760000
ICESTR33	30	2300	0.011	0.04	0.0615	2760000
ICESTR33+	120	2300	0.0115	0.04	0.0615	2760000
ICESTR34	60	2300	0.013	0.04	0.0615	2760000
ICESTR34+	120	2300	0.0135	0.04	0.0615	2760000
			0.011			
ICESTR35	30	469.2	0.0165	0.04	0.0615	563000
ICESTR35+	60	469.2	0.017	0.04	0.0615	563000
ICESTR36	30	565.8	0.0057	0.04	0.0615	679000
ICESTR36	30	493.35	0.0085	0.04	0.0615	592000
ICESTR36+	30	476.1	0.0115	0.04	0.0615	571000
ICESTR37	120	565.8	0.00593	0.04	0.0615	679000
ICESTR37	60	565.8	0.00593	0.04	0.0615	679000
ICESTR38	120	476.1	0.011	0.04	0.0615	571000
ICESTR38	60	476.1	0.011	0.04	0.0615	571000
ICESTR39	120	493.35	0.0087	0.04	0.0615	592000
ICESTR39	60	493.35	0.0087	0.04	0.0615	592000

+ Rubble accumulation collected for these tests only.

* Estimated value based on previous empirical work on similar material.

3.1.1 Rubble accumulation analysis: selection of method

Given this unique opportunity to directly examine a product of ice-structure interaction, careful consideration of the possible methods of observation was necessary. Factors influencing this decision included a desire to maximize the information obtained and to fully examine parameters of interest, which included: piece size, porosity, and angle of repose of the pile.

Initially, non-destructive testing of the rubble accumulations was considered. This would have been ideal, as the sample would remain intact for further analysis if this were later deemed to be necessary. This consideration led to the investigation of two methods: laser profiling and mould making.

Laser profiling, by assembling a series of two-dimensional slices, would have yielded a reconstruction of the shape of the rubble pile. This data could then be used to determine overall rubble pile geometry. There were several challenges associated with this method. A problem is presented by the material properties of the ice itself. The reflection coefficient is high, and much of the energy sent to the surface of the ice rubble cone by the laser is scattered. This results in a limited range of the laser equipment, which leads to increased difficulty in producing accurate scans. Secondly, when attempts were made to coat the ice with a smoother surface, the temperature sensitivity of ice became a factor for consideration. Because of the low temperatures required, simple solutions such as matte finish paint were eliminated. Encasing the sample in plastic was attempted, but a reliable seal could not be obtained to hold the covering in place. Additionally, the need for precise imaging (including some piece size measurements and accurate section location) made this method impractical. Using laser profiling, porosity or multiple piece size measurements, two highly desirable types of data, could not be obtained. As a result, laser profiling was rejected as a technique to examine the ice rubble piles. Other methods were considered due to lack of information regarding the rubble pile's internal structure.

Mould making was considered as a possible augmentation of the laser profiling method. If a cast of the ice rubble pile could be produced in a material, then perhaps a more coherent signal could be generated by the laser profiler, and the value of the laser profiling method could be retained. Again, the temperature sensitive nature of ice presented a challenge, as most powder casting agents, i.e. plaster of paris, are exothermic during the setting process - producing heat as they crystallise. This characteristic of casting agents is not acceptable as it would result in sample degradation, in the form of melting and/or recrystallisation. A search for an appropriate medium did not yield any readily available, inexpensive, reliable materials. As a result, this method was abandoned as a technique to examine the ice rubble piles.

3.1.2 Thin sectioning of centrifuge rubble accumulations

After thorough examination of the preceding non-destructive testing methods, destructive methods which would permanently alter the samples were examined. The first method involved producing thick sections by cutting slices approximately 10 mm thick. A smooth surface was created by sublimation. Polarising sheets were then used to obtain an approximate outline of the crystal structure. The second proposed method was thin sectioning, which is much more time consuming, but is correspondingly more precise. An imitation sample was created from ice grown in a cold room at 1 g and analyzed using both thick and thin sectioning. The thin sectioning was found to be the method capable of giving the most information in the smallest number of sections, and was more accurate

than the thick sectioned test case. Included as Figure 3. 3 is a photograph illustrating the properties of an idealized thin section of an ice rubble cone.

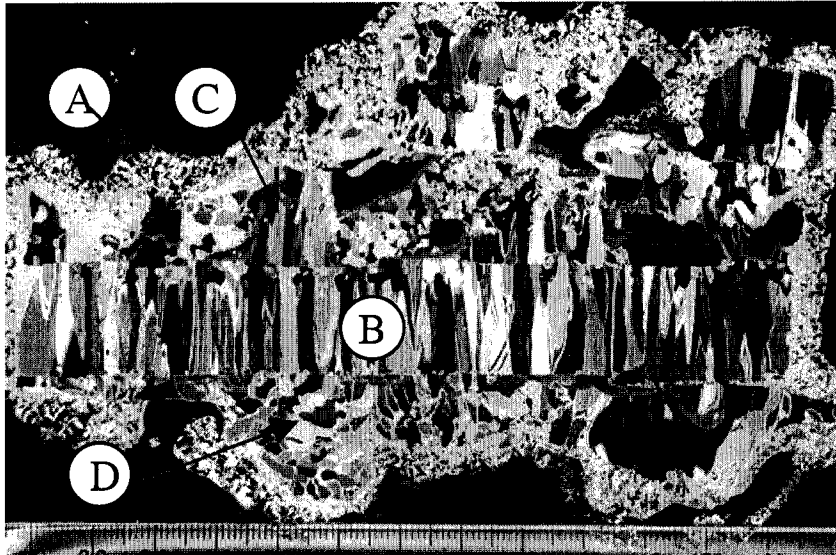


Figure 3. 3: Illustrative sample thin section.

The section is illuminated from behind and placed between polarizing sheets oriented at 90 degrees to one another. The scale is marked along the bottom of the photo in mm. The black areas represent areas of no ice.

A - The border around the overall shape of the section, made up of many tiny ice crystals, is created by the water used to weld the section to the glass slide it is mounted on.

B - The level ice, which runs across the photo horizontally, is of the S2 type and the crystals which compose it can be seen thickening downward.

C & D - Several macroscopic collections of ice crystals, representing a given piece of ice rubble, can be observed in the section. The orientation of these pieces can be distinguished on the basis of the cross section produced: if the grains are viewed as columns (C), the piece has been sectioned in the vertical plane; if the grains are viewed as a group of polygons (D), the piece has been sectioned in the horizontal plane. The outside dimensions of the rubble pieces are also visible.

This thin section provided a variety of information about the internal geometry of the sample. It allowed the measurement of the rubble pile's macroscopic properties, i.e. the

angle of repose of the ice rubble. For these reasons, thin sectioning was adopted as the method of analysis for the ice rubble cones produced in the centrifuge test series.

The process required to produce a thin section is outlined briefly, followed by a description of the selection of the critical sections for each ice rubble cone. Thin sections were produced in a cold room using a combination of equipment from both machining and biological disciplines which were cooled to below freezing. To minimize sample degradation, the work was at an average temperature of -10°C .

The ice rubble cone was measured and photographed. Approximate cut locations were marked on the cone in felt tip marker. A bandsaw was then used to produce approximately 10 mm thick sections through the sample. It was especially important to note location of the section which was of particular interest within the sample, because the final section had a thickness of only 0.5 mm. The thick section was affixed to a glass slide and was polished to a smooth surface by microtoming; this smoothed side was then affixed to another glass slide and the first one was removed. The sample thickness was then reduced to the required 0.5 mm by a combination of bandsaw and microtome use depending on temperature, salinity, and fragility of the sample. The result is a section as seen in Figure 3. 3.

The selection of the placement of such cross-sections in the ice rubble cone is crucial to truly developing a good understanding of the ice-structure interaction process. Initially, the co-ordinate system proposed used the x, y, and z axes as they are labelled in a

centrifuge package (x = vertical, y = horizontal in the plane of the g-field, z = horizontal perpendicular to the plane of the g-field). However, as the sectioning process developed, this proved cumbersome and a radial co-ordinate system was developed. Each section was labelled ICESTR###i###dfdt, where each of the label segments is as explained in Table 3. 4:. The first cone sectioned (ICESTR34) uses a different labelling system. An outline of sectioning schemes, locations, and labelling can be found in Appendix A.

Table 3. 4: Labelling scheme for thin sections

Alphabetic centrifuge test code	ICESTR
Numerical centrifuge code	2 digits
Number of section completed for a given rubble cone	Lower case Roman numerals i.e. iii
Angular measurement (0-360°, measured clockwise from direction of structure travel)	2-3 digits i.e. 45
Short form of 'degrees from direction of travel' or 'parallel to direction of travel'	dfdt or ptdt

3.2 ICE TANK DATA

In January of 2000, an extensive series of tests was conducted at IMD involving the interaction of level ice sheets with upward breaking conical structures. This author did not participate in this testing program; however, undertook an extensive review of the resulting video footage. Data available from the ice tank is the most extensive and standardized of any of the three testing methods covered in this thesis. Several cameras recorded each episode of ice-structure interaction. Data analysis in the case of the IMD data consisted of thorough reviews of these video records and noting the typical sequences of events during a trial. Conditions in the ice tank were also the most

homogeneous of any of the test cases. See Table 3. 5 for summary of IMD test conditions.

Table 3. 5: IMD test series summary

TEST CODE	g-level	flexural strength (kPa)	h (m)	V (m/s)	W/2 or 'r' (m)	E (kPa)
C45_V0P01_R1_001	1	37	0.0338	0.01	0.615	41700
C45_V0P01_R2_003	1	37	0.0338	0.01	0.615	41700
C45_V0P01_R3_005	1	34.5	0.0338	0.01	0.615	41700
C45_V0P05_R4_007	1	35.9	0.0338	0.05	0.615	41700
C45_V0P10_R5_009	1	34.5	0.0338	0.1	0.615	41700
C45_V0P25_R6_011	1	33.6	0.0338	0.25	0.615	41700
C45_V0P50_R7_013	1	32.9	0.0338	0.5	0.615	41700
C45_V0P005_R8_014	1	30.4	0.0338	0.005	0.615	41700
C45_V0P01_R9_022	1	16.8	0.0338	0.01	0.615	41700
C45_V0P01_R10_024	1	17	0.0338	0.01	0.615	60400
C45_V0P01_I55_073	1	27	0.0521	0.01	0.615	60400
C45_V0P10_I55_075	1	26.9	0.0521	0.1	0.615	60400
C45_V0P20_I55_077	1	26.8	0.0521	0.2	0.615	60400
C45_V0P01_I55_079	1	31.4	0.0521	0.01	0.615	60400
C45_V0P05_I55_081	1	31.2	0.0521	0.05	0.615	60400
C45_V0P10_I55_083	1	31.1	0.0521	0.1	0.615	60400
C45_V0P25_I55_085	1	31	0.0521	0.25	0.615	60400
C45_V0P50_I55_087	1	30.9	0.0521	0.5	0.615	60400
C45_V0P005_I55_089	1	33	0.0521	0.005	0.615	60400
C45_V0P01_I55_097	1	31	0.0521	0.01	0.615	60400
C45_V0P10_I55_099	1	28	0.0521	0.1	0.615	60400
C45_V0P20_I55_101	1	28	0.0521	0.2	0.615	60400
C45_V0P01_I83_026	1	43	0.081	0.01	0.615	226900
C45_V0P01_I83_028	1	42	0.081	0.01	0.615	226900
C45_V0P01_I83_030	1	39.4	0.081	0.05	0.615	226900
C45_V0P05_I83_032	1	44.1	0.081	0.1	0.615	226900
C45_V0P10_I83_035	1	43.7	0.081	0.25	0.615	226900
C45_V0P25_I83_038	1	43.3	0.081	0.5	0.615	226900
C45_V0P50_I83_041	1	42.7	0.081	0.005	0.615	226900
C45_V0P005_I83_044	1	42.5	0.081	0.01	0.615	226900
C45_V0P01_I83_047	1	35	0.081	0.01	0.615	226900
C45_V0P01_I83_050	1	33	0.081	0.01	0.615	226900
C45_V0P01_I110_053	1	33	0.1151	0.01	0.615	224000
C45_V0P01_I110_055	1	41	0.1151	0.01	0.615	224000
C45_V0P01_I110_057	1	40.3	0.1151	0.05	0.615	224000
C45_V0P05_I110_059	1	39	0.1151	0.1	0.615	224000
C45_V0P10_I110_061	1	38.5	0.1151	0.25	0.615	224000
C45_V0P005_I110_067	1	37.4	0.1151	0.01	0.615	224000

C45_V0P01_I110_069	1	36.5	0.1151	0.01	0.615	224000
C45_V0P01_I110_071	1	34	0.1151	0.01	0.615	224000
C60_V0P01_I55_104	1	49	0.0339	0.01	0.615	78500
C60_V0P01_I55_108	1	34.7	0.0339	0.025	0.615	78500
C60_V0P025_I55_110	1	35	0.0339	0.05	0.615	78500
C60_V0P05_I55_112	1	34.3	0.0339	0.1	0.615	78500
C60_V0P10_I55_114	1	37	0.0339	0.25	0.615	78500
C60_V0P0025_I55_122	1	33.9	0.0339	0.01	0.615	78500
C60_V0P01_I55_124	1	30	0.0339	0.01	0.615	78500
C60_V0P01_I110_126	1	37.3	0.1169	0.01	0.615	203000
C60_V0P01_I110_128	1	35.3	0.1169	0.05	0.615	203000
C60_V0P05_I110_130	1	34.9	0.1169	0.1	0.615	203000
C60_V0P10_I110_132	1	34.5	0.1169	0.25	0.615	203000
C60_V0P005_I110_138	1	33.6	0.1169	0.0025	0.615	203000
C60_V0P0025_I110_140	1	33.1	0.1169	0.001	0.615	203000
C60_V0P001_I110_142	1	32.6	0.1169	0.15	0.615	203000
C60_V0P15_I110_144	1	31.9	0.1169	0.2	0.615	203000
C60_V0P20_I110_145	1	31.8	0.1169	0.01	0.615	203000
C60_V0P01_I110_146	1	27	0.1169	0.01	0.615	203000
C60_V0P25_I110_134	1	34.2	0.1169	0.5	0.615	203000
C60_V0P50_I110_136	1	33.9	0.1169	0.005	0.615	203000
C60_V0P25_I55_116	1	36.5	0.0339	0.5	0.615	78500
C60_V0P50_I55_118	1	36	0.0339	0.0025	0.615	78500
C45_V0P25_I110_063	1	38	0.1151	0.5	0.615	224000
C45_V0P50_I110_065	1	37.7	0.1151	0.005	0.615	224000

3.3 PROTOTYPE DATA

The dynamic process of ice-structure interaction was observed at the Confederation Bridge in the Northumberland Strait in March of 2001. The Confederation Bridge is subjected to sea ice forces annually between approximately December and March. Velocity of the passing pack ice is principally influenced by the semi-diurnal tidal cycle and by wind. Pier geometry and average ice thicknesses are given in Section 2.2. A monitoring program is in place at the bridge to gather ice force data. The conditions in the Strait at the time of the field program were 90% or greater ice cover with 30% of the

ice classified as medium first year ice (0.7-1.2 m thick) and the remainder of the ice classified as thin first year ice (0.3-0.7 m thick) according to the Canadian Ice Service (CIS) ice chart for the region. See Table 3. 6 and Table 3. 7 for a summary of prototype interaction events. Note that flexural strength and E are estimated from Williams (1996) and h, V, and R were estimated to the best of the ability of the observers based on experience, comparison with benchmark objects, and the timebase of the observations once video was obtained. Procedures for these estimates are included in subsequent sections.

Table 3. 6: Prototype non-rubbling events observed during field program, spring 2001.

Event number	g-level	flexural strength (kPa)	h (m)	V (m/s)	W/2 or 'r' (m)	E (kPa)	floe radius R (m)
1	1	300	0.75	0.35	7.05	500000	16
2	1	300	0.75	0.45	7.05	500000	14
3	1	300	0.75	0.45	7.05	500000	2
4	1	300	0.75	0.35	7.05	500000	9
5	1	300	0.75	0.25	7.05	500000	5
6	1	300	0.75	0.3	7.05	500000	15
7	1	300	0.75	0.35	7.05	500000	2
8	1	300	0.75	0.35	7.05	500000	10
9	1	300	0.75	0.35	7.05	500000	5
10	1	300	0.75	0.35	7.05	500000	4
11	1	300	0.75	0.35	7.05	500000	26
12	1	300	0.75	0.35	7.05	500000	5
13	1	300	0.75	0.35	7.05	500000	11
14	1	300	0.75	0.35	7.05	500000	11
15	1	300	0.75	0.35	7.05	500000	8
16	1	300	0.75	0.25	7.05	500000	16
17	1	300	0.75	0.25	7.05	500000	7
18	1	300	0.75	0.25	7.05	500000	15
19	1	300	0.75	0.25	7.05	500000	4
20	1	300	0.75	0.45	7.05	500000	18
21	1	300	0.75	0.35	7.05	500000	8
22	1	300	0.75	0.35	7.05	500000	4
23	1	300	0.75	0.35	7.05	500000	5

24	1	300	0.75	0.35	7.05	500000	6
25	1	300	0.75	0.35	7.05	500000	10
26	1	300	0.75	0.35	7.05	500000	8
27	1	300	0.75	0.35	7.05	500000	15
28	1	300	0.75	0.35	7.05	500000	11
29	1	300	0.75	0.35	7.05	500000	7
30	1	300	0.75	0.35	7.05	500000	6
31	1	300	0.75	0.35	7.05	500000	8
32	1	300	0.75	0.35	7.05	500000	14
33	1	300	0.75	0.35	7.05	500000	13
34	1	300	0.75	0.35	7.05	500000	5
35	1	300	0.75	0.35	7.05	500000	5
36	1	300	0.75	0.35	7.05	500000	10
37	1	300	0.75	0.35	7.05	500000	6
38	1	300	0.75	0.35	7.05	500000	3
39	1	300	0.75	0.35	7.05	500000	4
40	1	300	0.75	0.45	7.05	500000	12
41	1	300	0.75	0.35	7.05	500000	7
42	1	300	0.75	0.45	7.05	500000	6
43	1	300	0.75	0.45	7.05	500000	7
44	1	300	0.75	0.45	7.05	500000	8
45	1	300	0.75	0.45	7.05	500000	4
46	1	300	0.75	0.45	7.05	500000	5
47	1	300	0.75	0.45	7.05	500000	20
48	1	300	0.75	0.45	7.05	500000	16
49	1	300	0.75	0.45	7.05	500000	27
50	1	300	0.75	0.35	7.05	500000	4
51	1	300	0.75	0.35	7.05	500000	6
52	1	300	0.75	0.35	7.05	500000	6
53	1	300	0.75	0.35	7.05	500000	17
54	1	300	0.75	0.45	7.05	500000	5
55	1	300	0.75	0.45	7.05	500000	7
56	1	300	0.75	0.45	7.05	500000	7
57	1	300	0.75	0.35	7.05	500000	11
58	1	300	0.75	0.35	7.05	500000	13
59	1	300	0.75	0.35	7.05	500000	9
60	1	300	0.75	0.35	7.05	500000	4
61	1	300	0.75	0.25	7.05	500000	11

Table 3. 7: Prototype rubbing events observed during field program, spring 2001.

Event number	g-level	flexural strength (kPa)	h (m)	V (m/s)	W/2 or 'r' (m)	E (kPa)	floe radius R (m)
1	1	300	0.75	0.35	7.05	500000	16
2	1	300	0.75	0.25	7.05	500000	18
3	1	300	0.75	0.4	7.05	500000	83
4	1	300	0.75	0.35	7.05	500000	70
5	1	300	0.75	0.3	7.05	500000	315
6	1	300	0.75	0.45	7.05	500000	34
7	1	300	0.75	0.45	7.05	500000	7
8	1	300	0.75	0.35	7.05	500000	26
9	1	300	0.75	0.35	7.05	500000	40
10	1	300	0.75	0.45	7.05	500000	21
11	1	300	0.75	0.45	7.05	500000	34
12	1	300	0.75	0.35	7.05	500000	37
13	1	300	0.75	0.3	7.05	500000	446
14	1	300	0.75	0.35	7.05	500000	74
15	1	300	0.75	0.35	7.05	500000	39
16	1	300	0.75	0.35	7.05	500000	10
17	1	300	0.75	0.35	7.05	500000	14
18	1	300	0.75	0.25	7.05	500000	14

3.3.1 Field data collection: selection of method

The on site observations were undertaken to supplement remotely acquired time-lapse video observations of ice rubble accumulation. The majority of the field observations consist of downward looking video above one of the piers typically seen in profile from the permanent observation cameras. Several axial and lateral rubble accumulation profiles were obtained using a laser range finder. Due to the vantage point of the observers, it was not possible to obtain exactly the same observations in the field as in the centrifuge; however, the process was generally found to be similar in the field when compared to the model testing program.

3.3.2 Field data: video analysis

Continuous video was shot using a Sony Mini-DV video camera. Segments of video were then selected from the eight hours of tape obtained and Adobe Premiere software was used to convert the video to a series of bitmaps. General observations regarding the process of ice rubble accumulation were supplemented by the ice rubble pile profiles, obtained using the laser range finder. Video segments corresponding to these profiles were used to calibrate the images. Timing of the profiles was apparent from the audio collected on the continuous video. The images corresponding to these times were used to determine the scale of the bitmap image. Each profile was benchmarked to the same starting point. The profiles provided distance to the rubble pile as ice surface as well as the angle of tilt. Data from the range finder was plotted, and the scale of the image calculated based on the size of the image, an object of a known size (the rubble pile) on the plane of interest, and the distance. This allowed the calculation of the scale of the image in terms of distance per pixel. This method does not correct for radial distortion; however, the important interactions were occurring near the center of the image. From the angle information obtained from the range finder, it is known that the video camera was positioned within $\pm 3^\circ$ of vertical.

To obtain ice velocity, individual ice features were tracked temporally and spatially through a sequence of frames collected at a known rate and the velocities observed were averaged. In the case of large floes, velocities were checked at several points during the

floe's interaction with the bridge piers. Velocity data were estimated and largely subdivided into 'fast' and 'slow', relative to the range of rates observed during the field program. There were no extreme velocity events during the period of observation, so the variation of ice speed was caused primarily by tidal currents and wind. The average velocities calculated from the video sequences agreed with Williams' average (1996) observed velocity of 0.23 m/s. Velocity estimates are approximately ± 0.05 m/s.

Ice thickness data was not recorded during the season of the field exercise, so only qualitative estimates of the ice thickness are available. Given the CIS chart, reasonable certainty can be used when classifying ice into 'thin' (less than 0.3 m), 'medium' (0.3-0.5 m) and 'thick' (0.5-1.0 m) categories. The floe sizes were estimated based on comparison of maximum floe dimension with the 250 m (centre to centre) span between bridge piers, accurate to ± 25 m. For floes passing the camera, the size was estimated based on approximate ice velocity multiplied by the time required for the floe to pass the pier.

Rubble pile footprint was estimated based on the sum of images with and without the rubble pile highlighted, using the distance per pixel scale factor described previously. Each set of frames was analyzed manually, thus excluding the possibility of algorithm problems in differentiating between level ice and rubble pile. An automated process would have permitted the detailed analysis of a larger number of interactions; however,

the relative stability of steady state rubble accumulations made it possible to obtain a representative sample by manual means.

4 EXPERIMENTAL RESULTS

4.1 CENTRIFUGE DATA

4.1.1 Qualitative observations – video

A small CCD camera with a wide-angle lens was mounted parallel to the axis of travel of the cone to record the process of ice structure interaction during centrifuge testing. Typical interaction events consisted of initial cracking, with large cracks that could be seen radiating throughout the ice sheet. These cracks were generally visible, especially in freshwater ice, because a large portion of the ice sheet was displaced upward on the order of a few millimeters. Following this initial failure, smaller pieces of ice formed, and in some cases ice rubble accumulation began.

In the case of freshwater ice, accumulation was often relatively rapid and the piece size approximately $1/10^{\text{th}}$ of the structure diameter or less. The accumulation was generally more than one ice thickness on the cone. The ice sheet was not observed to fail in downward flexure as the accumulation on the level ice sheet increased in volume. In the case of saline ice-structure interaction events, the deformation mechanism of the ice sheet was much more ductile than that observed for freshwater ice sheets. Ice rubble did not accumulate. Piece size was larger, with most pieces framed by circumferential and radial cracks. The ice sheet appeared to lift as the model passed, and reform following passage of the cone, with only the cracks indicating that disturbance of the ice sheet had occurred.

4.1.2 Quantitative observations – thin sections

The ability to see the internal structure of a product of ice-structure interaction has revealed several interesting and unexpected observations. It was hoped that by measuring properties such as the angle of repose and determining the ‘grain size distribution curve’ for ice rubble piles, some of the debate about the nature of ice rubble as a material would be resolved. In addition, understanding of the mechanisms by which ice rubble piles form and (once formed) deform could be increased. The most significant finding from the thin sections obtained in this study is that local failure of an ice sheet is associated with ice rubble production and accumulation. This is visible in Figure 4. 1 and Figure 4. 3 at the point of contact between the level ice sheet and the cone.

The parent ice sheets in this study were both freshwater and saline. Three of the cones that were thin sectioned were freshwater (ICESTR 32, ICESTR 33, and ICESTR 34). Two of the cones that were thin sectioned were saline (ICESTR35 and ICESTR36). Angle of repose was only measured in cases where the accumulation of ice rubble formed a pile. Rubble piling did not occur in the saline test cases. This lack of a rubble pile has previously been observed in level ice testing in large testing basins such as that at IMD (Lau, 2000; McKenna and Spencer, 1994).

Both internal and external ice rubble pile geometry can be determined by examination of the thin sections produced. Measurements obtained include an estimate of porosity, angle of repose, and piece size. One measurement which was taken, but was not expected, was

the grain angle from vertical. This relates to the angle with the vertical made by the individual ice crystals in the level ice sheet as it rides up the cone. As the cone is a 45° angle for these tests, it would be expected that flexural failure would be the dominant mechanism which caused the ice sheet to fail. The grains of ice within the level ice sheet would be perpendicular to the cone surface or 45° to the vertical. This was not always the case, as is illustrated by section ICESTR32iv270dfd (Figure 4. 1). Table 4. 1 summarizes the measurements obtained for each of the sections produced.

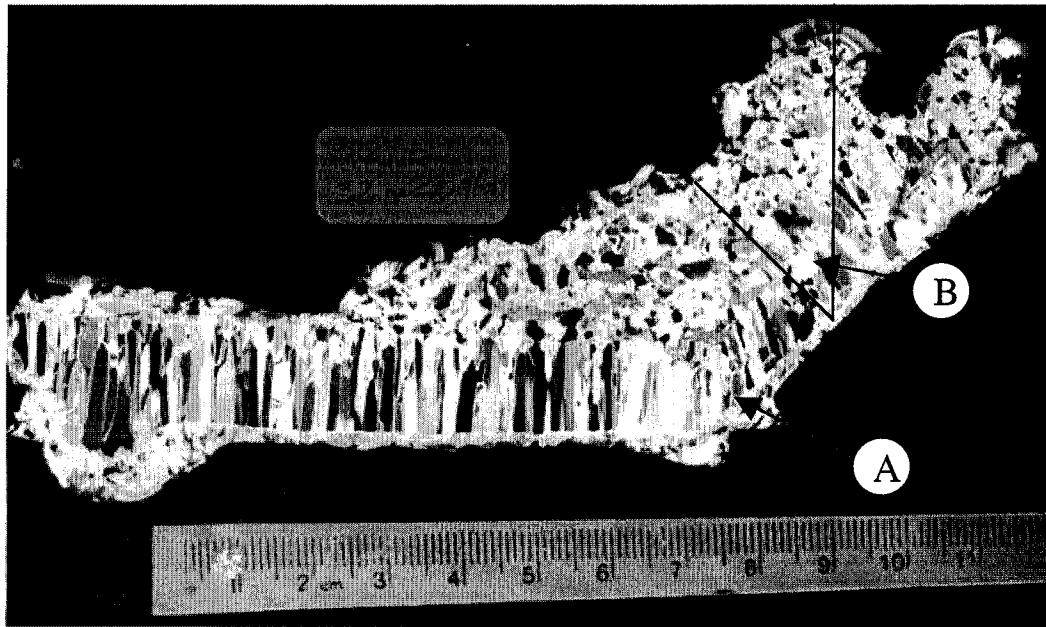


Figure 4. 1: Crossed polar view of ICESTR32iv270dfd. Illustrates the deformed nature of the level ice sheet grains at the ice-structure interface (A) and the location of the grain angle from vertical measurement (B). Scale divisions in mm.

Table 4. 1: Centrifuge thin section properties

Sample	Section	Angle of Repose, °	Approx. Porosity	Piece Size	Grain Angle from Vertical, °	Pile Region
ICESTR32 (freshwater)	i45dfdt	21	<5%	Macro	45	Upper
					0	Lower
	iiptdt	31	<5%	Mixed	35	
	iii235dfdt	27	<5%	Micro	N/A	
	iv270dfdt	29	<5%	Mixed	18	
	v315dfdt	27.5	<5%	Mixed	45	Upper
					20	Lower
ICESTR33 (freshwater)	iptdt	no pile	<5%	Mixed	N/A	
	iiptdt	34	~5%	Mixed	N/A	
	iiiptdt	21	<5%	Mixed	Varied	
	iv315dfdt	24	<5%	Mixed	45	
	v270dfdt	28	<5%	Mixed	45	
	vi225dfdt	27	<5%	Micro	N/A	
ICESTR34 (freshwater)	XZ, Y=0	25	<5%	Mixed	18	
	XZY1	28	<5%	Mixed	35	
	XZY2	no pile	N/A	Micro	N/A	
	XY, Z=15	25	<5%	Mixed	15	Upper
	XY, Z=28a	no pile	<5%	Mixed	N/A	
	XY, Z=28b	no pile	<5%	Mixed	N/A	
ICESTR35 (saline)	i270dfdt	no pile	no pile	Macro	35	
	ii315dfdt	no pile	no pile	Macro	45	Upper
					0	Lower
	iiiptdt	no pile	no pile	Macro	45	Upper
					0	Lower
	ivptdt (+20mm)	no pile	no pile	Macro	0	
ICESTR36 (saline)	iptdt	no pile	no pile	Macro	N/A	Lower
	ii45dfdt	no pile	no pile	Macro	45	Upper
					0	Lower
	iii90dfdt	no pile	no pile	Macro	45	

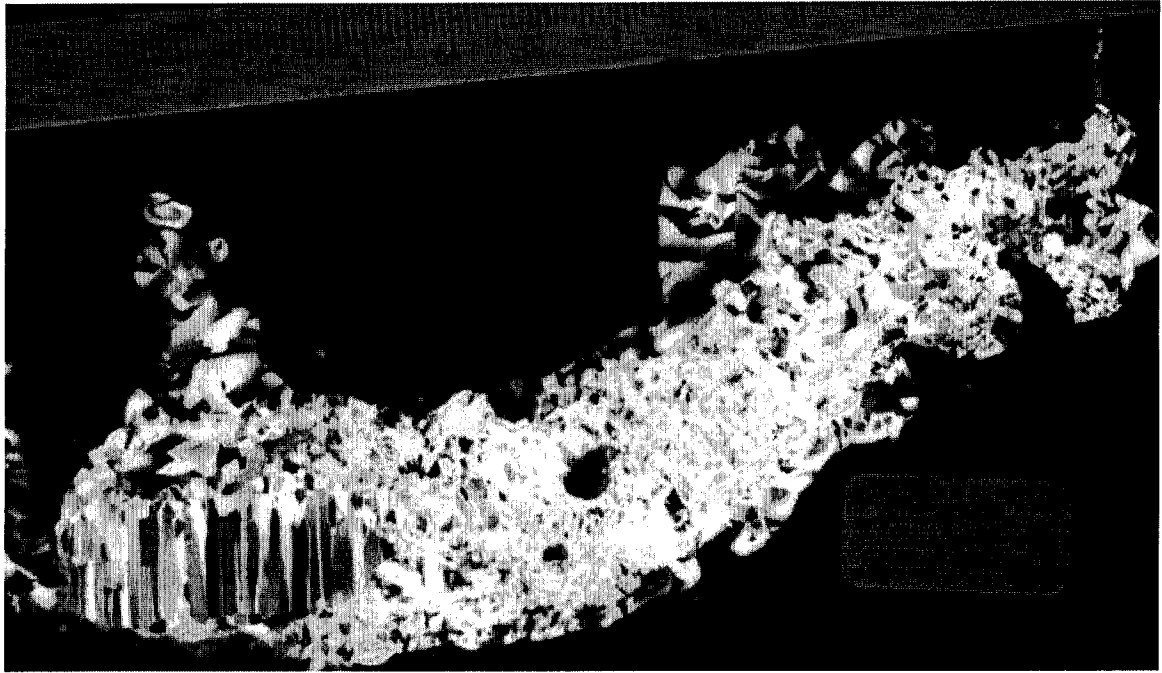


Figure 4. 2: Crossed polar view of ICESTR32iii235dfdt. Illustrates the small piece size of rubble in the clearing zones of the pile. Scale divisions in mm.

Ice rubble piece size was generally observed to be small in the freshwater cones which have been sectioned. The debris-like nature of the pieces can be clearly seen in sections such as ICESTR32iii235dfdt (Figure 4. 2). These sections are parallel or subparallel to the direction of travel of the cone, but along the profile of the cone, instead of perpendicular to the edge of the cone. The pieces seen on the saline cones were bounded by circumferential and radial cracks. This type of outlining is not seen in the freshwater cones sectioned. The cracks which formed in freshwater tests could be seen in the video to extend to the walls of the strongbox; in the saline ice sheets, the cracks may have extended as far but the behaviour of the ice sheet was not indicative of this (more ductile

deformation, no significant displacement of the ice sheet observed in the regions far from the model structure).

Thin sections provide insight by capturing in 'freeze frame' some of the mechanisms by which ice rubble piles deform. Short circuiting, whereby the ice rubble does not travel along the ice/cone interface to the maximum height of the rubble pile before it begins to add to the lateral extent of the pile, has been observed in several thin sections. The best example can be seen in section ICESTR33iiiptdt (Figure 4. 3), which illustrates the process by which the level ice sheet is being redirected over the piece of ice rubble nearest the top of the cone, as well as several triangular wedges of material that indicate this process has occurred repeatedly. There were no recorded occurrences of this type of phenomenon in the saline cones sectioned.

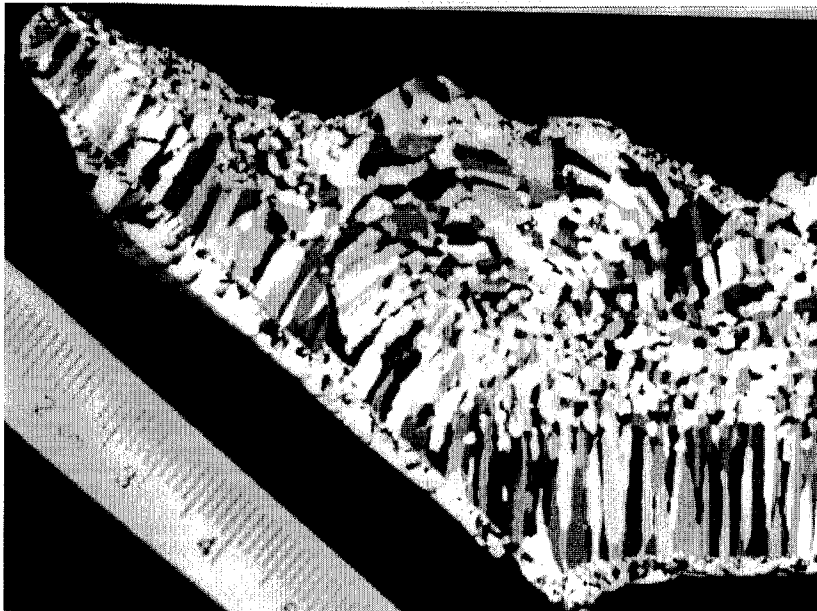


Figure 4. 3: Crossed polar view of ICESTR33iiptdt. Illustrates the short-circuiting of rubble pieces along a pathway which leaves an inactive zone at the top of the rubble pile. Evidence that this is a continuous process can be found in the 'roll over' structure in this section, composed of triangular rubble pieces in the centre right of the section.

4.1.3 Thin section method – data considerations

The possibilities that become available to the researcher when examining ice-structure interaction by this technique are many and varied. However, the method has limitations, and there are several issues of which one must be aware.

The advantage of the thin section method is that the internal structure of the ice and any associated ice rubble accumulation becomes visible to the investigator, by a snapshot obtained of the conditions within the ice-structure system. In the case of the centrifuge, the arresting of the motion of the structure happens within seconds, so deceleration effects should be minimal. Conversely, the thin sections provide a static view of a

dynamic process. This should be foremost in the mind of the investigator when drawing conclusions from this type of observation. Among the disadvantages of this method are the difficulties associated with storage of the sample and confidence that the sample has not undergone change while in storage, such as recrystallisation. Attempts to minimize such effects included bagging of samples and storage at low temperatures ($\sim -20^{\circ}\text{C}$). The sections do not exhibit unexpected ice crystal geometries in the level ice areas, which are well understood by modellers. This increases confidence that the samples were not altered during the storage period.

The use of polarized light makes it difficult to estimate porosity in some areas of the section, where black areas may be interpreted as either empty space or as a grain of ice oriented in such a way that it inhibits the passage of light. Additionally, there may be liquid water entrained in the sample at the time of collection, which subsequently freezes and thus decrease the porosity estimate. The small size of many of the ice rubble pieces, on the scale of one to a few grains (several mm), instead of the macroscopic pieces expected (10s of mm), makes this difficult to distinguish. However, section 32iv270dfdt (Figure 4. 1) is an illustrative example of where porosity can be positively identified and estimated.

4.1.4 Thin section observations – discussion

A proposed explanation for the granular deformation seen in the thin sections obtained in this study, which principally occurs in the lower area of the section where the level ice first contacts the cone, is that the ice deforms along grain boundaries to accommodate the shear forces exerted during the interaction process. Lau *et al.* (2000) observed that small piece size is associated with the shear failure mode. In other model tests, shear failure is associated with increasing loads. Once the ice rubble has been generated, the maximum height which the pile will reach becomes a statistic of interest to the researcher, as has been discussed by Mayne and Brown (2000). The process of short-circuiting may be related to some combination of variables which are also related to probability or extent of rubble pile formation.

4.2 ICE TANK DATA

The ice tank has been extensively used to model ice structure interaction processes; however, it has been noted that rubble piling as defined in this thesis is rarely if ever observed in the ice tank, even when additional ice pieces are placed at the beginning of an interaction event (McKenna and Spencer, 1994). One explanation may be low friction co-efficients, but this parameter is the same in both the centrifuge and the ice tank, and piling is observed in the centrifuge. If the model proposed in this thesis could explain this phenomenon, it would be of interest for many ice researchers.

4.2.1 Qualitative observations – process description

Failure of the EG/AD/S CD ice sheet around a conical structure typically consists of the following sequence of events:

- (i) bending of the ice sheet as it contacts the structure;
- (ii) formation of a circumferential crack at some distance from the cone (at the point of maximum bending stress);
- (iii) formation of radial cracks as the ice sheet is pushed up the cone; and
- (iv) sliding of the rubble blocks (formed by intersecting radial and circumferential cracks) off the cone once they are perpendicular to the direction of travel of the cone.

The whole process often appears as a smooth progression, and there may be occasional deposition of a few blocks on the level ice surface, but not a rubble pile as defined in this thesis. In a previous series, researchers attempted to produce rubble in a variety of ways, including piling broken ice around the cone before the interaction was started. However, even this did not produce a rubble pile (McKenna *et al.*, 1994).

4.3 PROTOTYPE DATA

4.3.1 Qualitative observations – process description

Events with no rubble accumulation were more common than rubble accumulation events. Ice rubble accumulation events were only observed for 14% of the time video was collected. Video was only collected during level ice interactions, so the total occurrence of ice rubble accumulations is even lower than 14%. In some cases, an

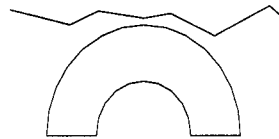
approximately triangular collection of various sized pieces of ice (typically less than 0.25 pier diameters) would occupy the zone usually associated with ice rubble accumulations directly in front of the pier causing incoming ice floes to be deflected away from the bridge piers. Non-rubble forming events also frequently occurred due to the discontinuous nature of pack ice as less energy was required to move a floe around the bridge pier than to initiate an interaction event. If a floe approached the bridge oblique to a pier, following the failure of a small portion of the ice against the bridge, it often pivoted around the point of first contact and cleared the bridge without further failure. When the direction of approach was perpendicular to the bridge, global failure by cracking often occurred instead of the development of an ice rubble accumulation. These patterns were observed for a variety of ice thicknesses, velocities, and floe sizes.

Rubble accumulation events were more likely if the floe was large (over ~100 m in diameter), or if a smaller floe was surrounded by other floes at the time it came in contact with the bridge pier. If ice rubble did begin to accumulate during the interaction of the bridge pier with a smaller floe, in the majority of cases, after the initial flexural failure of the ice sheet and a small zone of ice rubble had formed, the floe would split and clear around the bridge pier without the formation of further visible fractures. Even in the case of large floes, once a significant portion of the floe has passed the structure, a transition from local (rubbling) failure to global (splitting) failure was commonly observed.

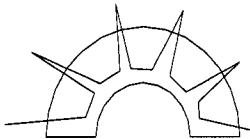
Ice rubble pile formation in the Northumberland Strait typically consists of the following sequence of events, Figure 4. 4:

1. The floe comes in contact with the bridge pier and fails in flexure, exhibiting both radial and circumferential cracking by forming several truncated wedges of ice which are pushed up and along the cone's surface. These wedges are macroscopic pieces, two to three ice thicknesses in the radial direction and approximately one ice thickness in width adjacent to the structure.
2. Following the formation of these truncated wedges, the ice rides up the cone and ice rubble forms. The piece sizes in this part of the interaction are much smaller than those formed during the initial stages, with maximum dimension on the order of one ice thickness or less.
3. The point of failure moves away from the ice-structure interface, leaving a inactive zone of rubble at the top of the pile near the structure. The active portion of the rubble pile continues to receive a supply of new ice pieces, material emerges from the border between the inactive and active zones and then cascades down to the leading edge of the rubble pile, extending out onto the incoming level ice sheet.
4. The pile's height and dimensions appear to reach steady state as the floe continues past the structure. Excess ice moves away from the side and rear of the pile. Failure of the level ice sheet due to some pre-existing flaw or by downward flexural failure may occur periodically. The process then returns to the upward breaking flexural failure and accumulation stages.

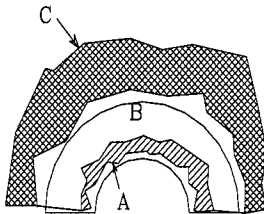
When a critical portion of the floe has passed the ice-structure interface, global failure in the form of a crack to the approaching edge of the floe will occur and the rubble pile will collapse.



Initial condition: floe approaching conical structure. Structure radius, r , small compared to maximum floe dimension, L .



Non-equilibrium ice rubble accumulation. Rubble piece size is large compared to r . Number of pieces is small.



Equilibrium ice rubble accumulation.
 A - inactive zone - quiescent, little movement is observed. Typically top $\frac{1}{3}$ of pile.
 B - active zone - pieces commonly emerge from top of zone and migrate to bottom. Usually bottom $\frac{2}{3}$ of pile.
 C - active level ice zone - downward flexural failure may occur; commonly ~ 1 pile dimension $(A+B)$ in front of structure.

Figure 4. 4: Typical Confederation Bridge level ice interaction sequence. Plan view of an upward breaking conical structure and an ice floe in various stages of interaction. Rubble accumulation represents local failure of the ice sheet. If a transition to global failure (splitting) occurs, it is usually after a significant portion of the floe has passed the bridge pier (more than 50% of the maximum floe dimension).

The effect of rubble accumulation beneath the level ice is recognized and influences the occurrence of downward flexural failure episodes, but the amount present is difficult to quantify from the video obtained. It is estimated from visual observations during this

field program that the porosity of rubble piles above the parent ice sheet is very low, contrary to previous field estimates that were on the order of 20 to 30 percent (Mayne and Brown, 2000).

An equilibrium ice rubble accumulation is shown in Figure 4. 5, which tracks the position of a dye balloon dropped onto a moving level ice sheet.

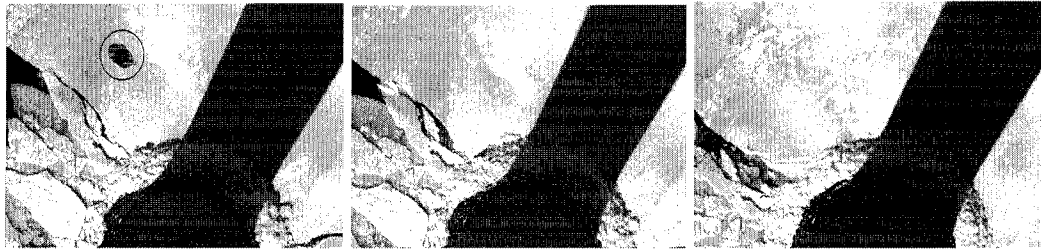


Figure 4. 5: Marker path during rubble accumulation event. Frames showing the path of dyed ice through a field ice rubble accumulation, verifying the short-circuiting pattern observed in the centrifuge. The direction of ice movement is approximately 45° , from the top left to the bottom right of the frame. The darkened area is the shadow cast by the pier on the ice.

This sequence of frames confirms that the short-circuiting process observed in the centrifuge model thin sections occurs in the field. The dye does not emerge at the apex of the rubble pile, but rather outside an inactive zone where very little movement of the constituent ice rubble pieces is observed. This zone typically comprises approximately the top one third of the pile footprint (nearest the bridge pier) in plan view.

4.3.2 Quantitative observations

Following extensive review of all the field observations, it was found that ice rubble initiation, accumulation, and dissipation processes are complex and are subject to a wide variety of parameters typical of natural systems. Analysis of these data was therefore not restricted to conventional variables such as velocity and ice thickness (see Chapter 5). Other variables, including the pile footprint and the percentage of the rubble pile composed of ‘macroscopic’ pieces (maximum dimension $\sim 0.1r$ to $\sim 0.2r$) were compared to rubble pile height. Pile footprint and piece size percentages were determined by subtraction of images. These observations are combined with the observed pile profile and angle(s) of repose to attempt to determine if a pattern could be identified in the circumstances of rubble pile formation. The centrifuge observations for freshwater ice rubble piles converted to prototype units were also plotted. Non-rubble events are under-represented because they are so common. In the field, there was no accumulation for all ice velocities with floe diameters below 25 m.

4.3.3 Field observations – discussion

Consistent with Mayne and Brown’s observations (2000), rubble piles did occur for the entire range of velocities observed for floes with diameters greater than 25 m. The number of observations obtained over a ten day period is small compared with entire seasons of data available to Mayne and Brown, so no commentary is included on the applicability of their proposed polynomial relationship between rubble pile height and velocity. The thickness data shown by Mayne and Brown registers nothing below 0.5 m.

This is likely a function of their method of measurement, but for reasons similar to those for the velocity relationship, no comparisons are made between this small subset of data and the wide range of data presented in their paper. No new trends linking particular conditions to ice rubble accumulation are immediately apparent from examining any of the plots included in Figure 4. 6. Points lying on the x-axis correspond to circumstances in the field where a level ice interaction did not result in the generation of a steady state ice rubble accumulation. In some cases, the floe pivoted and went around the pier; in others, the floe failed by splitting after a short period of contact with the structure.

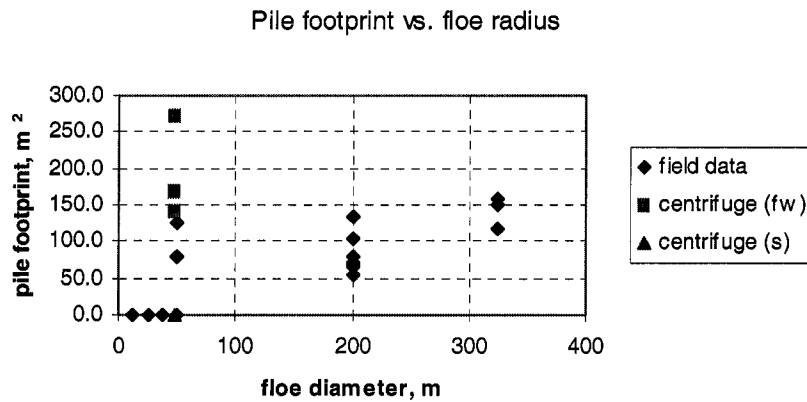
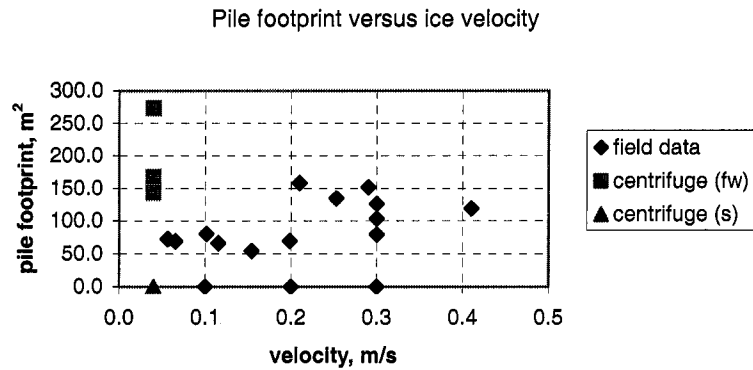
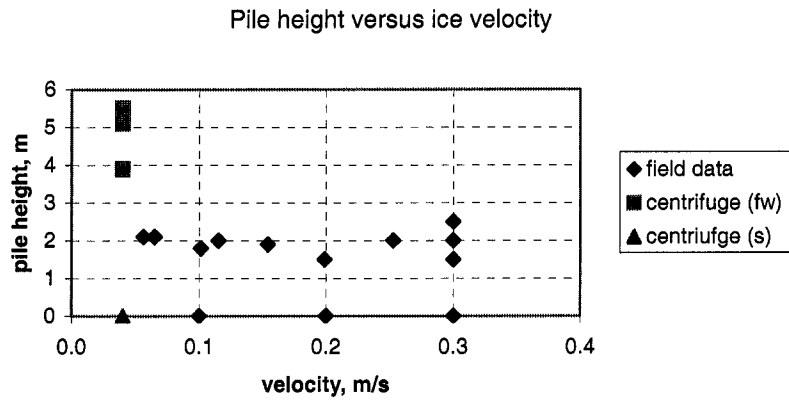


Figure 4. 6: Examination of video data quantified in terms of pile geometry. Ice rubble accumulation observations for field and freshwater centrifuge rubble accumulations. Centrifuge observations have been converted to prototype units. Cases of zero areas or pile heights correspond to non-rubble accumulation cases. (fw) denotes a freshwater ice sheet; (s) denotes a saline ice sheet.

The most important and consistent observation obtained in the field was that interactions with large floes or with small floes constrained by their neighbours resulted in ice rubble accumulation. In an attempt to isolate a possible size effect from a velocity effect, a plot of floe size vs. floe velocity was constructed for all the level ice-structure interactions observed during the field program (Figure 4. 7), showing rubble and non-rubble events. If a velocity limit exists for the process of ice rubble accumulation, a vertical demarcation between rubble and non-rubble events would exist on the plot. Similarly, if a floe size limit exists for the process of ice rubble accumulation, a horizontal demarcation should be apparent. Immediately obvious is the large number of non-rubble events compared to rubble events, and not all of the non-events observed are represented on the plot (due to incomplete recording of non-rubble events, which did not allow an assessment of floe size). Though there is some overlap between rubble and non-rubble conditions, a floe size limit of approximately 20 m for rubble accumulation was observed during this field program. No velocity limit is apparent for the range of data plotted; however, the range of ice velocities observed was not extensive. In no case did the ice rubble accumulation exist for the entire floe diameter – failure always occurred by global fracture after some portion of the floe had passed the structure. Figure 4. 8 details the ratio of the length past/length remaining for all the ice rubble events observed during the field program. There does not appear to be a consistent value of this ratio at which the failure mode transition occurs from local (rubbling) to global (non-rubbling/cracking).

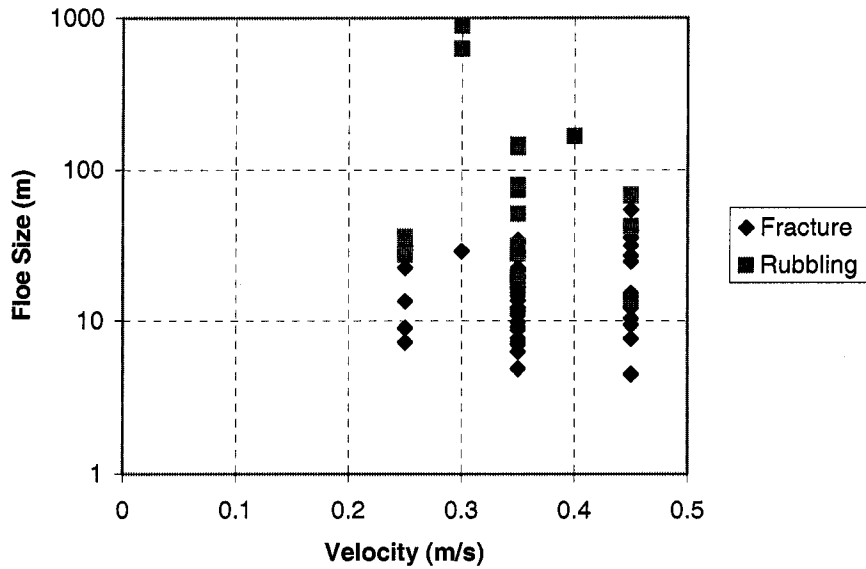


Figure 4. 7: Floe size versus floe velocity for field program observations. For the observations available, a size limit of approximately 20 m defines the minimum floe diameter for which an ice rubble accumulation will be observed.

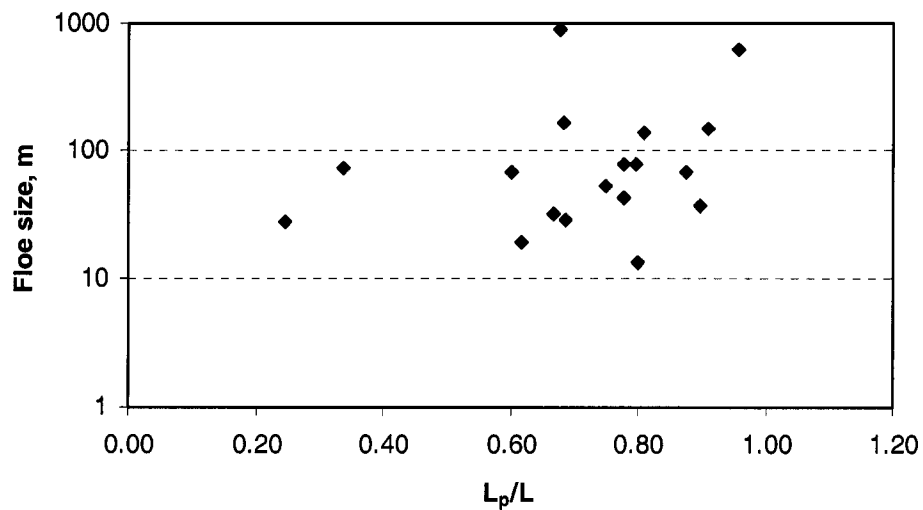


Figure 4. 8: Transition to global failure plotted relative to floe size. The ratio of floe length which has passed a structure (L_p) to the total floe length (L) remaining at the time of transition from an equilibrium rubble accumulation to global failure of the floe by fracture.

5 DISCUSSION

5.1 COMPARISON OF FIELD AND MODEL OBSERVATIONS

5.1.1 Field and ice tank observations

The initial phases of interaction in the field and the ice tank are similar. Both begin with the development of truncated wedges of broken ice as the structure comes in contact with an ice floe. After this point, the results of the interaction diverge. In the field, the floe will split or rubble; in the ice tank, the most common outcome is the formation of a single layer of ice pieces on the surface of the cone. At high velocities and thicknesses, a spray of small pieces may accumulate in front of the structure (Lau *et al.* 2000), but this ‘rubble pile’ lacks the active and inactive zones which characterize field rubble accumulations. The piece size distribution in the ice tank is not typically well graded, usually consisting of either mostly large or small pieces. In the field a wide range of piece sizes is observed.

5.1.2 Ice tank and centrifuge observations

5.1.2.1 Freshwater centrifuge tests and ice tank tests

Essentially the same differences exist between freshwater centrifuge tests and ice tank tests which exist between the field and the ice tank. As in the field, during the initial phase of interaction, the processes look similar but this similitude breaks down when an equilibrium situation is established. The behaviour of freshwater ice sheets in the centrifuge is very similar to that of saline ice in the field.

5.1.2.2 Saline centrifuge tests and ice tank tests

Observations of ice-structure interaction in saline centrifuge tests and ice tank tests are very similar. In both cases, a single layer of large pieces forms initially and no transition to a regime of smaller pieces and an ice rubble accumulation is generally observed. The saline centrifuge tests were only conducted at one velocity, so the opportunity did not exist to check for the transition to very uniform small pieces at high velocities in the saline centrifuge condition as was observed in the ice tank.

5.1.3 Field and freshwater centrifuge observations

These two cases exhibit the highest degree of similarity of any of the combinations examined in this thesis. Ice rubble accumulations were seen in both cases. In the field, ice rubble accumulations did not form in all interactions, but a correlation does appear to exist between increased floe size and increased probability of ice rubble accumulation. In all the freshwater ice sheets tested in the centrifuge, ice rubble did accumulate. This may be a function of boundary conditions imposed by the centrifuge strongbox, which could be equivalent to a large floe in the field case (apparent increased floe size). In addition to the incidence of ice rubble accumulations, the processes once accumulation has begun are similar in the freshwater centrifuge and field cases. Both circumstances develop well-graded rubble piles with distinctive active and inactive zones.

5.1.4 Comparison of physical observations with numerical model assumptions

The observations from both the centrifuge freshwater tests and prototype conditions show that once rubble piles have initiated, a transition to a shear failure mode is observed. The parent ice sheet does not continue to feed under the entire rubble accumulation and produce uniformly sized pieces which cascade down from the top of the rubble pile. Instead, small pieces produced by shearing at the ice-structure interface emerge from the active zone and the top of the rubble pile remains inactive (Figure 4. 4). This process is substantially different from the process on which the flexural failure models in Section 2.1.6 are based. Croasdale (1994) and Nevel's (1992) numerical models assume that the ice sheet fails in flexure, and that the level ice sheet is pushed up the cone and emerges at the top. The force calculation depends on these assumptions. On the other hand, the flexural numerical models do not account for the forces required to produce continuous shearing, or for the energy consumed in the shear deformation of the rubble pile. Lau *et al.* (2000) investigate the possibility of shear failure for a number of cases, and predict smaller pieces which are more similar to observations for the field and centrifuge freshwater ice.

Instead, it is likely that most force is required to shear the rubble and level ice at the boundary between the active and inactive zones. Most importantly, upward flexural failure does not appear to be the dominant mechanism of failure for steady state ice rubble accumulations. Equally important is the evidence from the field observations which show that not all ice-structure interactions result in ice rubble accumulations. This

has lead this author to examine other methods, such as Bhat's fracture mechanics analysis, to predict the incidence of ice rubble accumulations.

5.2 FRICTION BASED ANALYSIS OF ICE RUBBLE ACCUMULATION

Gershunov's paper (1987) outlines a condition under which a piece of ice may become trapped against a conical structure (see Section 2.5). His analysis is based on an unconsolidated rubble field interacting with an upward breaking conical structure, and uses a simple force balance in a polar co-ordinate system to predict whether or not rubble pieces will move up the cone. The result is a calculation of a critical friction co-efficient for a given geometry. The analysis assumes no self-weight of the ice pieces (if any) above a given piece of rubble, and in assuming that a rubble field is passing the cone, that there is no lateral component of the driving force on the rubble field near the cone. This is clearly not the case if a level ice sheet is interacting with a conical structure.

The field observations do not suggest that existing purely mathematical approaches such as those of Gershunov (1987) can accurately predict circumstances under which ice rubble will accumulate. If Gershunov's (1987) analysis were definitive, then theoretically the occurrence of rubble would depend only on the friction co-efficient between ice and the structure surface and the structure angle. However, in the field, there are clearly other factors that must be considered given the fact that rubble was only observed in some ice-structure interactions. In addition, the friction co-efficient of the piers of the Confederation Bridge are likely on the order of 0.1-0.2 for ice and rough

concrete depending on the velocity of interaction (Frederking and Barker, 2001). This is well below Gershunov's (1987) derived threshold of 0.58 for structures at 60°. In addition, the friction co-efficients of the IMD and centrifuge structures did not vary, yet the incidence of ice rubble accumulation was not consistent. Friction co-efficients were reasonably similar at all scales of testing (Lau *et al*, 1988; Barrette *et al*, 1999). Friction may explain the initiation of ice rubble piling (by Gershunov's force balance or some other means), but it does not provide a stand alone explanation for the process of ice rubble accumulation, particularly once an equilibrium condition has been reached.

5.3 FRACTURE MECHANICS APPLIED TO ICE RUBBLE ACCUMULATION

The field program made clear the true complexity of the prediction of ice rubble accumulation events. Any explanation of ice rubble accumulation events must also be consistent for non-accumulation events and the failure mechanism of a given ice floe in contact with the bridge piers. Fracture mechanics was investigated following the suggestion of a critical energy pathway solution – that the floe always fails in the manner requiring the least energy, and under some circumstances, this pathway includes ice rubble accumulation.

An ice floe in contact with a structure on one edge and being driven against this obstacle by wind or current can be thought of as a disc under uniaxial tensile load. Hallam (1986) outlines two conditions that will lead to failure in an uncracked sample of ice: crack nucleation and crack propagation. According to Hallam (1986):

“If the crack propagation stress is exceeded before the crack nucleation stress then failure is governed by the stress to nucleate a crack and the failure is very brittle. If, on the other hand, the stress to nucleate cracks occurs before the stress to propagate them, the failed ice will contain many cracks and will appear to show some ductility which is due entirely to the reduction in stiffness caused by crack nucleation. Final failure in this case is governed by the crack propagation stress.”

The process of an ice floe failing against a conical structure and either resulting or not in ice rubble accumulation is an extension of these conditions. Ice rubble will form when the failure is initially by crack nucleation, and global failure by splitting without formation of ice rubble will occur when failure is by crack propagation (Hallam, 1986).

Bhat *et al.* (1991) develop this idea in the outline of two possible scenarios for the failure of an ice floe in contact with a rigid vertical indenter. The floe is assumed to be a thin circular disk in inertia-driven motion comprised of an elastic-brittle material that obeys the Drucker-Prager failure criterion. The ice may fail locally (i.e. adjacent to the structure, resulting in formation of a rubble pile), or globally (i.e. by initiation of a large crack, resulting in floe splitting and passing around the structure). Bhat *et al.*'s (1991) analysis is compatible with Palmer's requirement of scaling of crack length (1991) because the crack length is relative to the whole floe. According to Bhat *et al.* (1991), the force required to initiate local failure is derived from the stress distribution around a semi-circular notch in combination with the Drucker-Prager failure criterion:

$$\alpha J_1 + J_2^{1/2} = K \quad (5.1)$$

where J_1 is the sum of principal stresses and J_2 is the second invariant of the deviatoric stress tensor. The material properties are functions of the ratios of uniaxial tensile (σ_t) and compressive (σ_c) strengths of ice:

$$\alpha = \frac{1}{\sqrt{3}} \left(\frac{m-1}{m+1} \right) \quad (5.2)$$

$$K = \frac{2m}{\sqrt{3}(m+1)} \sigma_t \quad (5.3)$$

Where $m = \sigma_c/\sigma_t$. (Note: for purposes of this study, σ_t is assumed to be equivalent to σ_f and that subsequent calculations are not sensitive to changes in this ratio, including a range of values between 6.5 and 8, as per 2.1.4.4). Taking $m = 2.5$ as the typical case, and $\sigma_{xx} \cong 0.73p$, $P_i = 2phr$ (where p is the incremental driving force, h is ice thickness, r is structure radius, and P_i is the force required to initiate rubble accumulation). Then the preceding equations reduce to

$$P_i = 2.06\sigma_f hr \quad (5.4)$$

From Bhat *et al.*'s (1991) FEM, the load required for floe splitting (where P_s is the splitting load, K_{IC} is fracture toughness, and R is the floe radius) is:

$$P_s = 0.62hK_{IC}\sqrt{2R} \quad (5.5)$$

For a particular structure radius, floe radius and set of material properties, the relative magnitudes of P_i and P_s indicate which failure mode will occur first as the contact force increases. The ratio of P_i to P_s can be expressed as

$$\frac{P_i}{P_s} = \frac{2.06 \times r \times \sigma_t}{0.62 \times K_{IC} \times \sqrt{2R}} \quad (5.6)$$

When $P_i/P_s > 1$, global failure is expected to occur before rubble accumulation. Based on the premise that ice rubble accumulation will only occur in combination with local failure, one can solve the above equation for the critical radius, R_{crit} , (when P_i/P_s is equal to one) which corresponds to the minimum radius for which ice rubble accumulation is expected. The ability of this formula to predict reasonable floe radii for rubble accumulation depends on the material property parameters input into the model. The values for fracture toughness and flexural strength vary over a wide range, depending on the temperature and salinity of the ice, along with loading rate. Values for K_{IC} and σ_f were sought from the literature as per Pfister *et al.* (2002) and are summarized in Table 5. 1.

Table 5. 1: Material properties of ice

	Flexural strength (kPa)	Fracture toughness (kPa \sqrt{m})	R_{crit} (m)
Field	300 *	79 *	3800
Centrifuge (freshwater)	1250 +	120 #	2.24
Centrifuge (saline)	500 +	80 **	0.81
Ice tank – weak ice, r=0.62 m	16.8%	3.23%	56.5
Ice tank – weak ice, r=0.48 m	16.8%	3.23%	34.4
Ice tank – strong ice, r=0.62 m	44.1%	6.72%	89.9
Ice tank – strong ice, r=0.48 m	44.1%	6.72%	54.8

*Williams (1993), + Barrette *et al.* (2000), # Dempsey (1989), ** Palmer (1991),
%IMD empirical relationship.

Although the results in Table 5. 1 represent idealized cases, they are consistent with observations in both centrifuge and field cases. In the field, confinement by adjacent

floes in heavy pack ice alters the stress distribution in the floe, producing the effect of a larger floe. Pre-existing flaws have the opposite effect by causing early fracture. No floe even approached the theoretical minimum radius of 3.8 km, but ice rubble accumulation was observed in approximately 14% of interactions seen in the field. The observations and the calculation both show that larger floes are more likely to produce rubble.

For saline ice in the centrifuge, the critical radius is approximately the dimension of the ice sheet in the strongbox. Once the interaction starts, ice fails locally and immediately, reducing the effective radius. Global failure in the form of a radial crack follows quickly. Subsequently, the ice fails in flexure as it rides up on the structure, and rubble formation is not observed.

More careful analysis is required for the case of freshwater ice in the centrifuge. Although the critical radius is much larger than the strongbox dimensions, local failure occurs and rubble accumulates. In fact, splitting failure, seen as large radial cracks on the video, always occurs near the beginning of the interaction. The ice sheet, constrained by the walls of the strongbox and too stiff to deform out of plane, continues to be held intact despite the presence of cracks and rubble formation follows. It is hypothesized that the strongbox acts like adjacent floes in the case of heavy pack ice in the field. The same mechanism is not effective in the case of the ice tank or in the case of saline ice in the centrifuge because the saline ice, with lower sheet modulus, deforms out of plane around the structure.

Treating the tendency to fail by fracture or to fail by rubble pile accumulation as a dimensionless ratio which integrates a material property (fracture toughness) should scale fracture correctly according to Palmer (1991). This implies that comparison of results from testing at different scales is possible by this method.

5.4 DIMENSIONAL ANALYSIS APPLIED TO ICE-RUBBLE ACCUMULATION

If friction and fracture mechanics alone cannot explain the incidence of ice rubble accumulation, other explanations must be sought. Dimensional analysis is commonly applied to phenomena which are complex in nature and for which isolating important variables in modeling is difficult. The method reduces the number of factors to consider by creating a series of dimensionless terms relating relevant independent variables.

5.4.1 Development of Model

One of the most crucial aspects of dimensional analysis is the initial selection of parameters which should include all variables of importance or suspected importance. The variables selected as relevant to this analysis are included in Table 5. 2, along with their units and nomenclature.

Table 5. 2: Rubble Pile Formation Factors.

Variables include elements of the geometry of an interaction event and material properties of ice.

Definition	Variable	Dimensional Units
Rubble pile height	P	L
Young's modulus (of ice)	E	$M T^{-2} L^{-1}$
Velocity of ice passing structure	V	$L T^{-1}$
Ice thickness	h	L
Waterline radius of structure	r	L
Flexural strength of ice	σ_f	$M T^{-2} L^{-1}$
Acceleration due to gravity	g	$L T^{-2}$
Density of ice	ρ_i	$M L^{-3}$
Density of water	ρ_w	$M L^{-3}$
Fracture toughness	K_{IC}	$M T^{-2} L^{-1/2}$
Floe radius	R	L

In this case, the rubble pile height is the dependent variable and all others contribute to it independent of each other. Young's modulus is included to account for the stiffness of the ice passing the structure. Velocity of interaction has been inferred to have importance in dictating the type of failure observed and the size of pieces observed as they break from the parent ice sheet. Ice sheet thickness, floe radius, and waterline structure radius are all relevant lengths in this problem. Floe radius is included due to the importance of this parameter in field observations. The flexural strength of the ice is included because it is a standard measurement available for most ice sheets and acts as an index for other ice strength parameters. Fracture toughness is included as a parameter of relevance to the minimum energy approach to prediction of ice rubble accumulation. The densities of ice and water are included to account for the buoyant weight of the ice and self-weight of ice rubble pieces. Gravitational acceleration is included because it is not constant at all scales.

Piece size is not included in the list of independent variables because it is not possible to specify the average piece size for a given ice sheet. The angle of the structure is not accounted for because the maximum height of the rubble pile should not be dependent on structure inclination if it is ninety degrees or less (Lau, 1999). The coefficients of friction between the ice and the structure and between the ice block surfaces are considered to be important. They are not, however, included in this iteration of the model as they are very similar in the ice tank and centrifuge and reasonably close to those in the prototype case.

Because of the large number of variables in this system, the matrix method (Sharp and Moore, 1983) was used to generate the following set of dimensionless Π terms:

$$\frac{P}{r} = \phi \left(\frac{E}{\sigma_f}, \frac{V^2 \rho_w}{\sigma_f}, \frac{h}{r}, \frac{gr \rho_w}{\sigma_f}, \frac{\rho_i}{\rho_w}, \frac{K_{IC}}{r^{1/2} \sigma_f}, \frac{r}{R} \right) \quad (5.7)$$

These terms can be compounded to the following form, which incorporates the Froude number:

$$\frac{P}{r} = \phi \left(\frac{E}{\sigma_f}, \frac{V^2}{gr}, \frac{h}{r}, \frac{\sigma_f}{gr \rho_i}, \frac{\rho_w - \rho_i}{\rho_w}, \frac{\sigma_f r}{K_{IC} R^{1/2}}, \frac{r}{R} \right) \quad (5.8)$$

This form has been adopted because it includes three standard dimensionless terms that are widely accepted in hydraulic and ice modelling. The Froude number, V^2/gr , is a ratio of inertial forces to gravity forces; E/σ_f is a strength index parameter commonly used in ice tanks; and $(\rho_w - \rho_i)/\rho_w$ accounts for the buoyant weight of the ice in a given test case. The P/r , h/r , and r/R ratios are clearly dimensionless and relate to the geometry of a given test case. This leaves $\sigma_f/gh\rho_i$, which combines the properties of the ice itself, the

self-weight of ice being displaced during the interaction process, and gravity. The fracture term, $\sigma_{fr}/K_{IC}R^{1/2}$, is very similar to the initiating versus splitting force ratio developed from Bhat *et al.* (1991) and relates the geometry of the structure, floe size and ice strength.

In the examination of this problem, there are two conditions. If $P/r > 0$, a rubble pile has formed and accumulation is occurring. If $P/r = 0$, no rubble pile has formed. From field observations, this condition suggests failure of the floe has occurred by splitting. If the 4 types of data available (centrifuge freshwater (fw), centrifuge saline (s), ice tank, and field) were divided into rubble ($P/r > 0$) and non-rubble ($P/r = 0$) cases by the series of dimensionless terms developed in the preceding section, it would be possible to state that some greater understanding of the process of ice rubble accumulation had been reached using this combination of variables. The following sections discuss the details of the available data and the assumptions made in each case, and summarizes the results of this model.

5.4.2 Ice Rubble Accumulation Cases

5.4.2.1 Prototype

For the purposes of this model, field data from the first-hand observations gained during the field program are used as inputs, in combination with data available in the literature. A much more comprehensive database of ice-structure interactions is available in the form of video recordings taken as part of the Confederation Bridge monitoring program;

however, these data are currently subject to a confidentiality agreement. When it becomes available, it would provide an excellent opportunity for further testing of this model.

As previously stated, the range of velocities observed during the field program was small in comparison with what has been observed over long periods (Mayne and Brown, 2000). No direct measurements were made of material properties during the field program, and subsequently all inputs for E , σ_f , and K_{IC} are taken from the literature. Values used in this model are listed in Table 5. 3. Ice thicknesses in the video data are available and were estimated in some cases. For the suite of interactions analyzed for incidence of rubble pile accumulation, however, these data on thickness were not isolated in the original analysis, so structure radius is used instead of ice thickness as the normalizing length in several of the Π terms. Floe size was inferred from the velocity and time required for the floe to pass a specified point. The inputs to the model could be enhanced through further analysis of the field data obtained. Structure radius is fixed at 7.05 m for the field case. This is a reasonable approximation as 14.1 m is the mean structure diameter over the course of a tidal cycle (Brown *et al.*, 1998). Field data were divided into rubbing ($P/r > 0$) and non-rubbing ($P/r = 0$) cases.

Table 5. 3: Variable values for prototype conditions

Variable	Value(s)	Source
E	500 MPa	Williams 1996
V	0.25 m/s – 0.45 m/s	Section 3.3
h.	0.25 m – 1.0 m, not measured specifically for the interactions listed	Section 3.3
σ_f	300 kPa	Williams 1996
K_{IC}	79 kPa m ^{1/2}	Pfister <i>et al.</i> 2002
R	2 m – 446 m	Section 3.3
r.	7.05 m	Brown <i>et al.</i> 1998

Eighteen rubbing events and sixty-two non-rubbing events were analyzed to obtain the values of the Π terms listed in Table 5. 4 and Table 5. 5.

Table 5. 4: Values of Π terms for prototype rubbing conditions

Π term	Minimum	Maximum	Average
E/σ_f	1667	1667	1667
$1000(V^2/gr)$	0.90	2.93	1.91
h/r	0.04	0.14	Not measured
$100(\sigma_f/gr\rho_i)$	0.48	0.48	0.48
$(\rho_w - \rho_i)/\rho_w$	0.12	0.12	0.12
$\sigma_f/K_{IC}R^{1/2}$	1.27	10.30	5.09
$1000(r/R)$	16	1044	307

Table 5. 5: Values of Π terms for prototype non-rubbing conditions

Π term	Minimum	Maximum	Average
E/σ_f	1667	1667	1667
$1000(V^2/gr)$	0.90	2.93	1.96
h/r	0.04	0.14	Not measured
$100(\sigma_f/gr\rho_i)$	0.48	0.48	0.48
$(\rho_w - \rho_i)/\rho_w$	0.12	0.12	0.12
$\sigma_f/K_{IC}R^{1/2}$	5.13	17.85	9.98
$1000(r/R)$	256	3133	1060

5.4.2.2 Ice Tank

Inputs for this model were taken from the test series conducted at IMD in January and February of 2000 by Lau. The test series used smooth cones at 45° and 60° in level ice. The results of the test series are reported in detail with respect to force comparisons and rubble processes by Lau *et al.* (2000). For all the test runs reported here no rubble accumulation formed. Because of the behavior of the ice sheet reported by Lau *et al.*, the trials in very thick ice at high velocities are not considered in this analysis because it is possible these circumstances resulted in a rubble accumulation of sorts. It is assumed for all ice tank tests reported that $P/r=0$. The floe radius was assumed to be half the ice tank width or 6 m. This is recognized as a lower bound for the radius, as it is likely that the effective radius is larger because the ice sheet was frozen to the sides of the tank. This assumption simplifies a rectangular testing basin to a circular one, in addition to assuming there are no significant boundary effects caused by the edges of the ice tank. The value of fracture toughness has been calculated from an empirical relationship developed by researchers at IMD. This relationship has been derived for convenience, as direct measurement of K_{IC} is complex. Despite this empirical relationship, it is assumed that σ_f and K_{IC} are independent inputs to the model. Well known standardized testing procedures assure quality input data for the model in the case of the ice tank. Density of the ice and fluid in the tank are well known. The facility's capabilities are also highlighted in the wide range of ice-structure interaction velocities tested. An explanation for the absence of rubble piles would assist in the accurate interpretation of

ice tank test results. The range of values for each variable in the model in the ice tank is listed in Table 5. 6.

Table 5. 6: Variable values for ice tank

Variable	Value(s)	Source
E	41.7 MPa – 227 MPa	Lau <i>et al.</i> 2000
V	0.001 m/s – 0.5 m/s	Lau <i>et al.</i> 2000
h.	0.034 m - 0.117 m	Lau <i>et al.</i> 2000
σ_f	16.8 kPa – 44.1 kPa	Lau <i>et al.</i> 2000
K_{IC}	3.23 kPa m ^{1/2} – 7.46 kPa m ^{1/2}	Empirical IMD relationship
R	6 m	Inferred
r.	0.48 m or 0.62 m	Lau <i>et al.</i> 2000

Sixty-two different runs in the ice tank were analyzed to obtain the values of the Π terms listed in Table 5. 7.

Table 5. 7: Values of Π terms for ice tank conditions (non-rubbling)

Π term	Minimum	Maximum	Average
E/σ_f	1127	7519	3960
$1000(V^2/gr)$	0.00	41	5.57
h/r	0.05	0.19	0.12
$100(\sigma_f/gr\rho_i)$	0.32	0.94	0.66
$(\rho_w - \rho_i)/\rho_w$	0.12	0.15	0.13
$\sigma_f/K_{IC}R^{1/2}$	1.31	1.65	1.60
$1000(r/R)$	103	103	103

5.4.2.3 Centrifuge

Rubble piling was observed and a pile height measurement made in all freshwater cases. Rubble piling was not observed for the saline tests. Values of the Π terms reported utilize actual radius or half the strongbox width of 0.4 m. It is unlikely that the strongbox walls create an identical boundary effect, but in both freshwater and saline tests, cracks were seen to propagate to the walls of the strongbox. This implies that the values of the Π terms reported are lower bounds. In the saline case, both E and σ_f drop by an order of magnitude (as compared to the freshwater values), leaving the value of the ratio unchanged and constant in both saline and freshwater cases. The range of variables for separate freshwater and saline cases and the corresponding values of the dimensionless Π terms in the proposed rubble piling model are listed in Table 5. 8, Table 5. 9, Table 5. 10, and Table 5. 11.

Table 5. 8: Variable values for centrifuge (freshwater)

Variable	Value(s)	Source
E	2760 MPa	C-CORE internal report
V	0.04 m/s	Lau <i>et al.</i> 2002
$h.$	0.011 m – 0.016 m	C-CORE internal report
σ_f	2300 kPa	C-CORE internal report
K_{IC}	120 kPa m ^{1/2}	Pfister <i>et al.</i> 2002
R	0.4 m	Barrette <i>et al.</i> 2000
$r.$	0.062 m	Lau <i>et al.</i> 2002

Table 5. 9: Variable values for centrifuge (saline)

Variable	Value(s)	Source
E	536 MPa – 679 MPa	C-CORE internal report
V	0.04 m/s	Lau <i>et al.</i> 2002
h.	0.006 m – 0.017 m	C-CORE internal report
σ_f	469.2 kPa – 565.8 kPa	C-CORE internal report
K_{IC}	80 kPa m ^{1/2}	Pfister <i>et al.</i> 2002
R	0.4 m	Barrette <i>et al.</i> 2000
r.	0.062 m	Lau <i>et al.</i> 2002

Table 5. 10: Values of Π terms for centrifuge freshwater (rubbling) conditions

Π term	Minimum	Maximum	Average
E/σ_f	1200	1200	1200
$1000(V^2/gr)$	0.02	0.09	0.05
H/r	0.18	0.26	0.21
$100(\sigma_f/gr\rho_i)$	3.5	14.1	7.2
$(\rho_w - \rho_i)/\rho_w$	0.10	0.10	0.10
$\sigma_f/K_{IC}R^{1/2}$	1.86	1.86	1.86
$1000(r/R)$	153.8	153.8	153.8

Table 5. 11: Values of Π terms for centrifuge saline (non-rubbling) conditions

Π term	Minimum	Maximum	Average
E/σ_f	1200	1200	1200
$1000(V^2/gr)$	0.02	0.09	0.05
h/r	0.09	0.28	0.16
$100(\sigma_f/gr\rho_i)$	0.71	3.40	1.85
$(\rho_w - \rho_i)/\rho_w$	0.09	0.09	0.09
$\sigma_f/K_{IC}R^{1/2}$	0.57	0.69	0.61
$1000(r/R)$	153.8	153.8	153.8

5.4.3 Model Results

Dimensional analysis of a complex problem such as ice rubble accumulation makes it possible to reduce the number of parameters under investigation and determine how these parameters are linked to the final result. However, in this particular case, where there are 8 dimensionless terms, relationships are more complex than they would be in situations with fewer terms, and the inter-relationships between the terms are more difficult to illustrate graphically. Each term is discussed individually, and then a series of figures are presented illustrating the inter-relationships between terms.

As stated in the introduction, variable selection is the most important part of model construction. Comparing the current analysis to that of Lau *et al.* (2000), a different definition of Froude number is required ($Fr=V/(gh)^{1/2}$). Average values of the Froude number for the case examined in this thesis as defined by Lau *et al.* (2000) are included in Table 5. 12.

Table 5. 12: Froude comparison, all test cases

Condition	Average Froude number ($V/(gh)^{1/2}$)
Centrifuge – freshwater ice, $P/r>0$	0.01 (all testing at one value of V)
Centrifuge – saline ice, $P/r=0$	0.02 (all testing at one value of V)
IMD ice tank	For large h, $V \rightarrow$ exceed 0.02
Field observations, $P/r>0$	0.11 – 0.23, depending on h
Field observations, $P/r=0$	0.12 – 0.23, depending on h

The criterion established by Lau *et al.* (2000) is that Froude scaling is important for Froude values in excess of 0.02. For the purpose of studying the incidence of rubbing processes, this threshold does not appear to differentiate between rubbing and

non-rubbling events. Froude number values, as defined in this study, are similarly indistinct. In addition to studying Froude values in isolation, the relationship between Froude number and the other proposed Π terms has been examined and fails to distinguish between rubbing and non-rubbling circumstances. The buoyant weight term, $(\rho_w - \rho_i)/\rho_w$, remained relatively constant in all cases, ranging from 0.09 to 0.15. For this reason, the effects of this term are considered to be minimal and are not investigated with respect to the remaining Π terms. No useful information would be expected to emerge from plotting the two aspect ratio terms against each other, so they are only compared with the more complex Π terms. The remaining Π terms (E/σ_f , $\sigma_f r/K_{IC} R^{1/2}$, and $\sigma_f/gr\rho_i$) have been considered as the most significant outputs of this model.

The stiffness term (E/σ_f) has only one value in the prototype case due to the non-specific but representative material property values input from the literature. In the IMD case, E is measured once for each ice sheet, and as σ_f changes with time and temperature, the value of the ratio changes. The prototype and centrifuge values are on the low end of the range of values seen at IMD. Rubble piles were not seen at IMD regardless of the range of E/σ_f studied, and rubble piles were not seen in saline centrifuge tests but were seen in freshwater centrifuge tests with the same E/σ_f value. This suggests that at least in this Π term alone there is not sufficient information to divide these data into rubble and non-rubble categories. It should be noted that the values of E and σ_f in the centrifuge are estimated.

The range of the $\sigma_f/gh\rho_i$ term is greater in the centrifuge than in the ice tank or prototype, indicating the effect of varying gravity. Similarly, in the case of the $\sigma_f/gr\rho_i$ term, a wide range of values is seen in the freshwater centrifuge case, and the remainder of cases (saline centrifuge, field, and ice tank) all have similar values grouped at the low end of the freshwater range. Therefore it is unlikely that this term contains the correct combination of variables to isolate incidents of ice rubble accumulation.

In prototype, for the rubbing condition, the fracture term ranges from 1.30 to 10.30, the average value is 5.09. For the non-rubbing condition, the fracture term ranges in value from 5.13 to 17.85, the average value is 9.98. In the ice tank, the fracture term values lie between 1.30 and 1.65. Saline centrifuge values vary in a narrow range between 0.57 and 0.69; freshwater centrifuge values are constant at 1.86. If the dimensionless term is thought of as a ratio of rubble pile initiating to floe splitting forces (similar to that derived in section 5.3), theoretically values of 1 and below would correspond to incidents of rubbing. A more loose interpretation, given the assumptions made for some of the input parameters, would be that lower values would be expected to be associated with rubbing and higher values with non-rubbing. The field data follows this pattern; however, inconsistencies emerge in the ice tank and centrifuge datasets.

The ice tank fracture toughness ratio value is comparable to the lower portion of the range of the field values, implying rubbing should occur but it is not observed. If the boundary effects of the ice tank have been underestimated and the tank walls create a

confined system or effectively larger ice floe, this is also inconsistent as it would only serve to decrease the ratio value further. A similar effect would result if the K_{IC} value calculated underestimated EG/AD/S CD ice fracture toughness.

In the centrifuge, the fracture toughness ratio is highest in the freshwater case which is at the low end of observed values in the field in instances of rubbling. This is at first encouraging, until the ratio is calculated for the saline ice sheets, where the value is lower than the smallest field value by a factor of 2. That non-rubbling events are associated with lower values of the fracture term ratio in the centrifuge is anomalous when compared with the field data where low values are associated with rubble accumulations.

Of all the parameters investigated, the fracture toughness term holds the most potential for explaining the combination of variables that result in ice rubble accumulation. Further investigation is recommended to better quantify the input parameters (especially material properties) and fully explore the potential of the proposed model. Plots of these data discussed in the previous section follow in Figure 5. 1, Figure 5. 2, Figure 5. 3, and Figure 5. 4. In each case, the fracture term is plotted on the abscissa and the other dimensionless terms on the ordinate. None of the plots reveal a definitive differentiation of these data between rubbling ($P/r>0$) and non-rubbling ($P/r=0$) cases. Note that apparent correlations are spurious due to the presence of the same variable in the dimensionless terms on both axes in several cases.

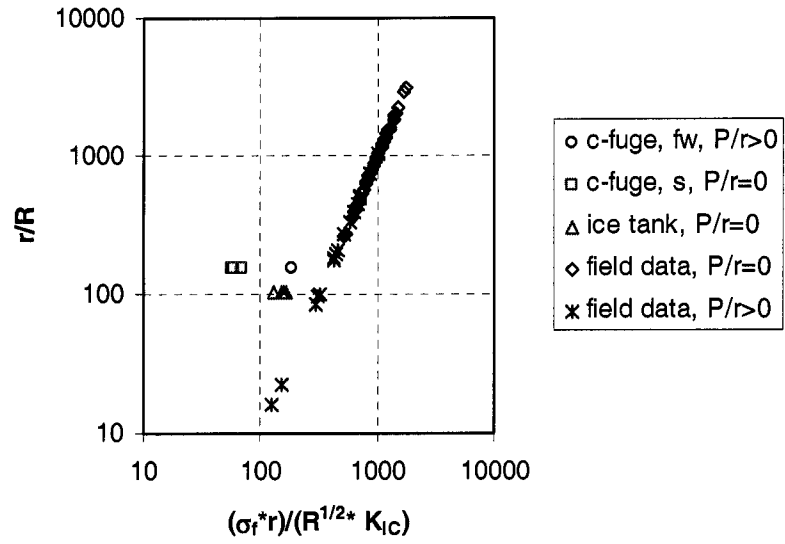


Figure 5. 1: Aspect ratio versus fracture toughness term.

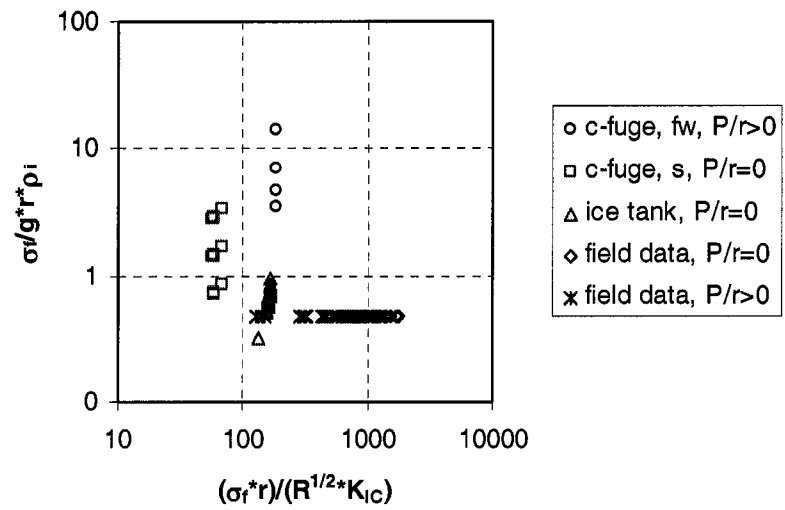


Figure 5. 2: Cauchy term versus fracture toughness term.

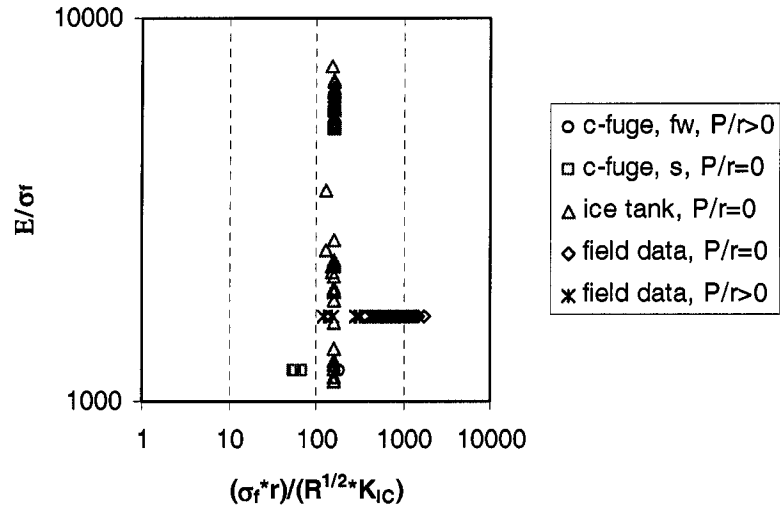


Figure 5. 3: Stiffness term versus fracture toughness term.

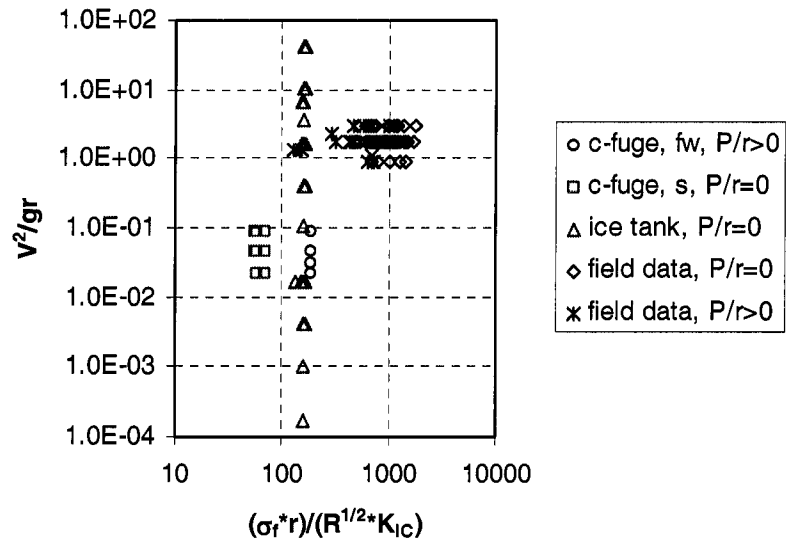


Figure 5. 4: Froude number versus fracture toughness term.

5.4.4 Implications

The process of ice rubble piling around conical structures has been associated with force maxima, and for this reason is of interest to researchers. Dimensional analysis has been applied to 11 independent variables relevant to this process, yielding 8 dimensionless Π terms. The values of these terms at various scales have been plotted and preliminary attempts to understand the implications of these terms have been made. This method provides a basis for data reduction and comparison from different sets of experiments, and could easily be expanded to incorporate future results.

5.5 FRACTURE MECHANICS AND DIMENSIONAL ANALYSIS

The thin sections obtained from centrifuge tests indicate that when ice rubble forms, it is as a result of local deformation of the ice sheet. Field observations confirmed this, and also showed that incidents without ice rubble accumulation are associated with global failure (splitting). These observations support Hallam's (1986) methodology, and this method is used in Bhat *et al.*'s (1991) calculation of force to fail a circular ice sheet.

The force ratio, P_i/P_s , was developed as a method of defining whether local or global failure was more likely to occur in a given interaction. However, the limitation of this analysis is its failure to consider the out of plane forces that will be associated with level ice interacting with a conical indenter. Because material properties such as E are inferred, not measured for each test evaluated by this method, if compliance is an issue, it will not be obvious from the values used. Though a promising methodology, when

examined in detail, the force ratio failed to consistently explain observed circumstances of rubble (local) and non-rubble (global) failures in the centrifuge, ice tank, and field. Dimensional analysis was chosen as a method of attempting to simplify the complex problem of ice-structure interaction. Fracture toughness was included as one of the variables in this analysis, and the Π term $\sigma_{fr}/K_{IC}R^{1/2}$ was developed. With the exception of a constant multiplier, this term is the same as the force ratio, P_i/P_s .

In order to compare the two methods, the ratio of critical radius to actual radius is tabulated below in Table 5. 13.

Table 5. 13: Ratio of critical to actual radii, all model conditions

	R_{act} (m)	R_{crit} (m)	R_{crit}/R_{act}
Field (average value) $P/r=0$	10	3800	380
Field (average value) $P/r>0$	72	3800	53
Centrifuge freshwater $P/r>0$	0.4*	2.2	5.6
Centrifuge saline $P/r=0$	0.4*	0.8	2.0
Ice tank $P/r=0$	6*	90	15
		34	6

*Observations suggest boundary conditions imposed by adfreezing to sides of tank makes this an upper bound.

One would expect rubbing to occur if R_{crit}/R_{act} is less than one, i.e. critical radius is less than the actual radius. The trend is correct for field values – decreasing R_{crit}/R_{act} values are associated with increasing probability of rubbing. The ratio also correctly predicts rubbing will not occur in the ice tank. However, higher values of R_{crit}/R_{act} in freshwater versus saline centrifuge tests is the reverse of what is observed – rubbing does occur in

freshwater tests and does not occur in saline tests. Further characterization of material properties in specific cases would add confidence that the findings made through the use of dimensional analysis and fracture mechanics make valuable contributions to understanding the process of ice-structure interaction.

6 CONCLUSIONS

An investigation of the process of ice rubble accumulation at three scales has been conducted. Centrifuge testing has shown agreement with prototype scale processes. This agreement is verified by reproduction of local failure mechanisms seen in thin sections in field observations collected at the Confederation Bridge. Commonalities include short-circuiting of equilibrium ice rubble accumulations in freshwater centrifuge tests and small piece size in freshwater ice rubble accumulations. Prototype observations showed that rubble pile accumulations were more likely during interactions with large ice floes. This association of ice rubble with large floe events is responsible for the correlation of force maxima with ice rubble accumulation. In interaction events observed at the Confederation Bridge which did not involve generation of ice rubble, ice floes consistently failed globally by splitting.

Given the above relationship, three theories were investigated as possible explanations for incidences of ice rubble accumulation. Gershunov's (1987) hypothesis of rubble pile initiation by friction arresting the motion of a piece of ice rubble on an inclined plane proved inadequate to explain the results of either the model or prototype conditions following quantification of the friction coefficients in these situations. An investigation of ice rubble accumulation from the perspective of minimum energy led to the examination of the theory of fracture mechanics. The methodology of Hallam (1986) and Bhat *et al.* (1991) was used to develop an equation which compared the force necessary to initiate ice rubble accumulation (local failure) to the force required to initiate floe splitting

(global failure). This ratio was solved at a critical value of one for the minimum floe radius which would be expected to produce ice rubble, substituting the appropriate material properties for ice from the literature. General trends indicate that larger floes would be more likely to rubble, which matches the field observations. Dimensional analysis of the ice-structure interaction process led to the definition of a dimensionless group that incorporated fracture toughness with interaction geometry and ice strength. Early results indicate that this term shows promise in differentiating cases of ice rubble accumulation versus cases of no ice rubble accumulation for field data but is not consistent in predicting the ice failure mechanism at all test scales.

Ice rubble accumulation was not predicted for the ice tank, and was not observed. Scaling of processes governed by fracture using Palmer's (1991) similitude criteria indicates that scaling of fracture must be done on the basis of the system rather than on the basis of a material property. The method of Bhat *et al.* (1991), in referencing crack length compared to floe size, incorporates this principle. The reasoning of Palmer (1991) also encourages the use of the fracture term from the dimensional analysis portion of this work as a method of comparing tests of different scales because the value of the term is also relative the system rather than the value of a material property.

Thin sections were made of ice rubble accumulations and deformed ice sheets from the centrifuge test series, and allow a unique perspective to be gained through seeing the internal structure of these accumulations. Rubble accumulation is associated with local

failure of the ice sheet, including deformation at the ice-structure interface. Piece size is generally small and the path of pieces through the rubble pile does not follow classic models of flexural failure where pieces remain in contact with the cone until they emerge from the top of the rubble pile. Instead, an equilibrium ice rubble accumulation usually consists of an active zone (near the incoming level ice sheet) which is fed by the approaching ice sheet, and an inactive zone, typically the top third of the rubble pile, which is a stagnant accumulation of ice blocks.

Recommendations for further work include better characterization of inputs to the fracture mechanics term of the dimensional analysis through investigation of material properties and integration of these data available from the Confederation Bridge monitoring program into the current model when it becomes available. Ice thickness data could be integrated and would further increase understanding of ice rubble accumulation processes.

7 REFERENCES

- Alexeev, Y.N. and Karulina, M.M., 1999. An Assessment of pile-up dimension in front of sloping offshore structures. *Proc. 15th International Conference on Port and Ocean Engineering Under Arctic Conditions*, Helsinki. V.1, pp.396-405.
- Arunachalam, A.V.M., 1996. Conditions for ice pressure and failure mode analysis during ice-structure interactions from dimensional analysis. *Proc. 6th International Offshore and Polar Engineering Conference*, Los Angeles.V.2, pp. 323-332.
- Barrette, P.D., Lau, M., Phillips, R., McKenna, R.F., and Jones, S.J., 2000. Interaction between level ice and conical structures: centrifuge simulations phase II. *Proc. 19th International Conference on Offshore Mechanics and Arctic Engineering*, New Orleans. OMAE paper 00-1004.
- Barrette, P.D., Phillips, R., McKenna, R.F., Jones, S.J., and Crocker, G., 1999. Interaction between level ice and a conical structure: centrifuge simulations. *Proc. 18th International Conference on Offshore Mechanics and Arctic Engineering*, St. John's. OMAE paper 99-1148.
- Barrette, P.D., Phillips, R., Clark, J.I., and Crocker, G., 1998. Physical properties of columnar ice grown in a centrifuge. *Proc. 8th International Offshore and Polar Engineering Conference*, Montreal. V.2, pp. 519-525.
- Bhat, S.U., Choi, S. K., Wierzbicki, T., and Karr, D.G., 1991. Failure analysis of impacting ice floes. *Journal of Offshore Mechanics and Ocean Engineering*. 113(2): 171-178.
- Brown, T.G., Croasdale, K.R., Bruce, J.R., and Azarnejad, A., 1998. Observations from the Confederation Bridge ice monitoring program. *Proc. 8th International Offshore and Polar Engineering Conference*, Montreal. V.2, pp. 438-443.
- Bruneau, S. E., 1996. Development of a First-Year Ridge Keel Load Model. Ph.D. thesis, Memorial University of Newfoundland. 307 pp.
- Cammaert, A. B., and Muggeridge, D. B., 1988. Ice Interaction with Offshore Structures. Van Nostrand Reinhold, New York, New York.
- Clough, H.F., and Vinson, T.S., 1986. Ice Forces on fixed conical structures. *Proc. 5th International Conference on Offshore Mechanics and Arctic Engineering*, Tokyo. V.4, pp. 507-514.
- Croasdale, K.R., Bruneau, S., Christian, D., Crocker, G., English, J., Metge, M., and

- Ritch, R., 2001. In-situ measurements of the strength of first-year ice ridge keels. *Proc. 16th International Conference on Port and Ocean Engineering Under Arctic Conditions*, Ottawa. V.3, pp.1445-1454.
- Croasdale, K.R., Cammaert, A.B., and Metge, M., 1994. A method for the calculation of sheet ice loads on sloping structures. *Proc. 12th IAHR International Symposium on Ice*, Tondheim, Norway. Volume 2 pp. 874-885.
- Enoki, K., Nakazawa, N., Ueda, T., and Saeki, H., 1990. Apparent friction coefficient between steel and ice under high contact pressure. *Proc. 10th IAHR International Symposium on Ice*, Espoo, Finland. V.2, pp. 902-911.
- Ettema, R., and Urroz, G.E., 1989. On internal friction and cohesion in unconsolidated ice rubble. *Cold Regions Science and Technology*, 16(3): 237-247.
- F. G. Bercha and Associates, 1987. Northumberland Strait Crossing Ice Climate Study: Final Report. Northumberland Strait Crossing Project, Public Works Canada.
- Frederking, R., and Barker, A., 2001. Friction of sea ice on various construction materials. *Canadian Hydraulics Centre Technical Report HYD-TR-67 PERD/CHC 3-49*.
- Gershunov, E.M., 1987. Structure-rubble field interaction. *Cold Regions Science and Technology*, 14(1): 95-103.
- Gilbert, R., 1997. GPHY 304 Arctic and Periglacial Environments: Course Notes. Queen's University at Kingston.
- Hallam, S.D., 1986. The role of fracture in limiting ice forces. IAHR working group Report – 3rd State of the Art Report. T.J.O. Sanderson. Hanover, NH, CRREL Special Report 87-17. 33 pp.
- Hoikkanen, J., 1985. Measurements and analysis of ice force against a conical offshore structure. *Proc. 8th International Conference on Port and Ocean Engineering under Arctic Conditions*. Narssarsuaq, Greenland. V.3, pp. 1203-1220.
- Izumiyama, K., Irani, M.B., and Timco, G.W., 1994. Influence of a rubble field in front of a conical structure. *Proc. 4th International Offshore and Polar Engineering Conference*, Osaka, Japan. V.2, pp. 553-558.
- Jones, S.J., Spencer, D., and McKenna, R.F., 1994. Icebreaking performance from Model Scale Tests. *Proc. ICETECH '94 (SNAME)*, Calgary, Canada. pp. H1-H19.

- Lau, M., Phillips, R., McKenna, R.F., and Jones, S.J., 2002. Modeling ice-structure interaction in a geotechnical centrifuge. *Proc. International Conference on Physical Modeling in Geotechnics*, St. John's. pp. 325:330.
- Lau, M., Jones, S.J., Phillips, R. and McKenna, R.F., 2000. Influence of velocity on ice-cone interaction. *Proc. IUTAM Symposium on Scaling Laws in Ice Mechanics and Ice*, Fairbanks, Alaska. pp. 127-134.
- Lau, M., 1999. Ice forces on a faceted cone due to the passage of a level ice field. Ph.D. thesis, Memorial University of Newfoundland. 384 pp.
- Lau, M., Williams, F.M., Molgaard, J., and Swamidass, A.S.J., 1999. An analysis of ice breaking pattern and ice piece size around sloping structures. *Proc. 18th International Conference on Offshore Mechanics and Arctic Engineering*, St. John's, Newfoundland, OMAE paper 99-1151.
- Lau, M., Muggerridge, D.B., and Williams, F.M., 1988. Model tests of downward breaking conical structures in ice. *Proc. 7th International Conference on Offshore Mechanics and Arctic Engineering*, Houston. V. 4, pp. 239-247.
- Lovell, M.S., and Schofield, A.N., 1986. Centrifugal modeling of sea ice. *Proc. 1st International Conference on Ice Technology*, Cambridge. pp. 105-113.
- McKenna, R.F., and Bruneau, S.E., 1997. Ice rubble build-up on conical structures during ridge interactions. *Proc. 16th International Conference on Offshore Mechanics and Arctic Engineering*, Yokohama, Japan. V.4, pp.355-364.
- McKenna, R.F., Bruneau, S.E., and Williams, F.M., 1996. In-situ shear strength measurements of model ice rubble using a punch technique. *49th Canadian Geotechnical Conference*, St. John's, Newfoundland. pp. 279-286.
- McKenna, R. F., and Spencer, D., 1994. Ice rubble buildup on conical structures. *Proc. 12th IAHR International Symposium on Ice*, Tondheim, Norway. V.1, pp.177-186.
- Määttänen, M., 1991. Ice Forces (Ch. 4 in *Offshore Structures*). Center for Marine Structures and Geotechnique, Florida Atlantic University. Boca Raton, FL.
- Määttänen, M. and Hoikkanen, J., 1990. The effect of ice pile-up on the ice force of a conical structure. *Proc. 10th IAHR International Symposium on Ice*, Espoo, Finland. V.3, pp. 1010-1021.
- Mayne, D. C. and Brown, T. G., 2000. Rubble pile observations. *Proc. 10th International Offshore and Polar Engineering Conference*, Seattle. V.1, pp. 596-599.

- Mellor, M., 1983. Mechanical behavior of sea ice. *U.S. Army Cold Regions Research and Engineering Laboratory*, 105p. United States. CRREL Report No: M 83-1.
- Mitchell, J.K., 1993. Fundamentals of soil behavior. John Wiley and Sons, Inc., New York, New York.
- Nevel, D.E., 1992. Ice forces on cones from floes. *11th IAHR International Symposium on Ice*, Banff. V.3, pp. 1391-1404.
- Palmer, A., 1991. Centrifuge modelling of ice and brittle materials. *Canadian Geotechnical Journal*, 28(6): 896-898
- Pfister, S., Williams, F.M., and Phillips, R. 2002. Interaction of level ice with upward Breaking conical structures at two scales. *16th IAHR International Symposium on Ice*, Dunedin, New Zealand. V.1, pp. 416-425.
- Phillips, R., Clark, J.I., Paulin, M.J., Meaney, R., Millan, D.E., & Tuff, K., 1994. Canadian national centrifuge centre with cold regions capabilities. *Proc. the International Conference Centrifuge 94*, Singapore. pp. 57-62.
- Schofield, A.N., 1980. Cambridge geotechnical centrifuge operations. *Geotechnique* 30(3): 227-268.
- Schwarz, J., Frederking, R., Gavrillo, V., Petrov, I.G., Hirayama, K.-I., Mellor, M., Tryde, P., and Vaudrey, K.D., 1981. Standardized testing methods for measuring mechanical properties of ice. *Cold Regions Science and Technology*, 4: 245-253.
- Sharp, J.J., and Moore, E., 1983. Partial analysis and matrix methods. *International journal of mathematical education in science and technology*, 14(4): 393-402.
- Sharp, J.J., 1981. Hydraulic Modelling. Butterworths, Toronto, Canada.
- Sinha, N.K., 1984. Intercrystalline cracking, grain boundary sliding, and delayed elasticity at high temperatures. *Journal of Materials Science*, 19: 359-376.
- Taylor, R.N. (Editor), 1995. Geotechnical Centrifuge Technology. Chapman & Hall, New York, New York.
- Timco, G.W., and O'Brien, S., 1994. Flexural strength equation for sea ice. *Cold Regions Science and Technology*, 22: 285-298.
- Timco, G.W., and Frederking, R.M.W., 1990. Compressive strength of sea ice sheets. *Cold Regions Science and Technology*, 17: 227-240.

- Wadhams, P., 2000. *Ice and the Ocean*. Gordon and Breach Science Publishers, Canada.
- Weeks, W.F., and Ackley, S.F., 1982. The growth, structure, and properties of sea ice. *U.S. Army Cold Regions Research and Engineering Laboratory*, 136p. United States. CRREL Report No: M 82-1.
- Williams, F.M., 1996. Ice features and ice mechanical properties in Northumberland Strait. *Proc. 6th International Offshore and Polar Engineering Conference*, Los Angeles. V.2, pp. 390-39.
- Williams, F.M., and Parsons, B.L., 1994. Size effect in the flexural strength of ice. *Proc. 13th International Conference on Offshore Mechanics and Arctic Engineering*, Houston, ASME: 15-22.

**APPENDIX A: THIN SECTIONS FROM CENTRIFUGE
TEST SERIES**

Test code: ICESTR32

Text conditions: 120g, ice thickness~11.5 mm, velocity 0.04 m/s

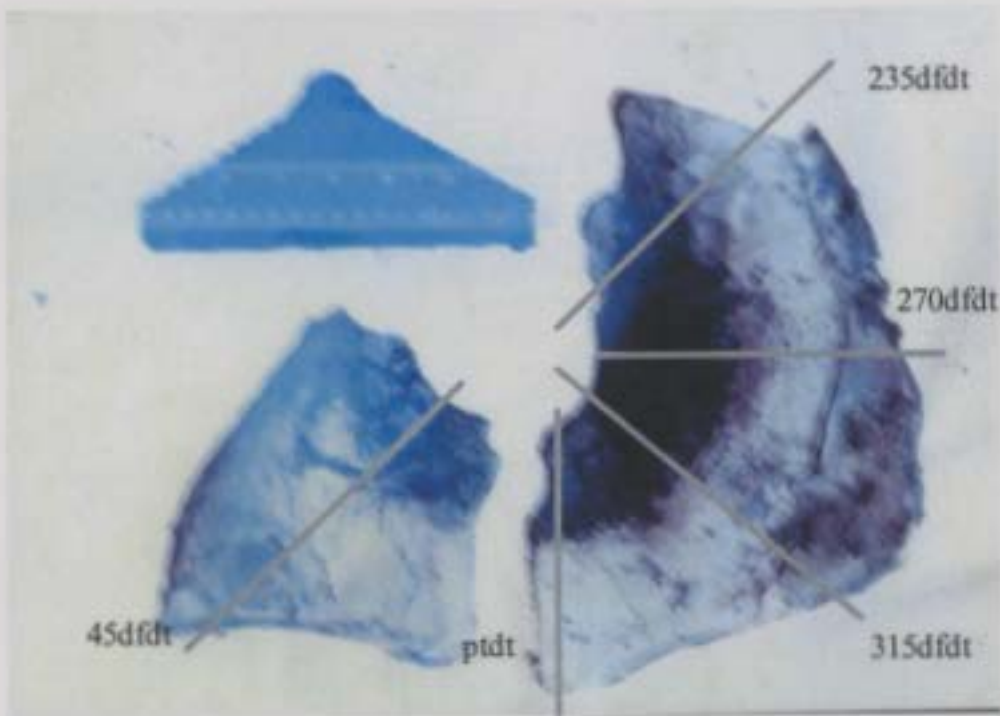


Figure 1: Section location outline – ICESTR32.

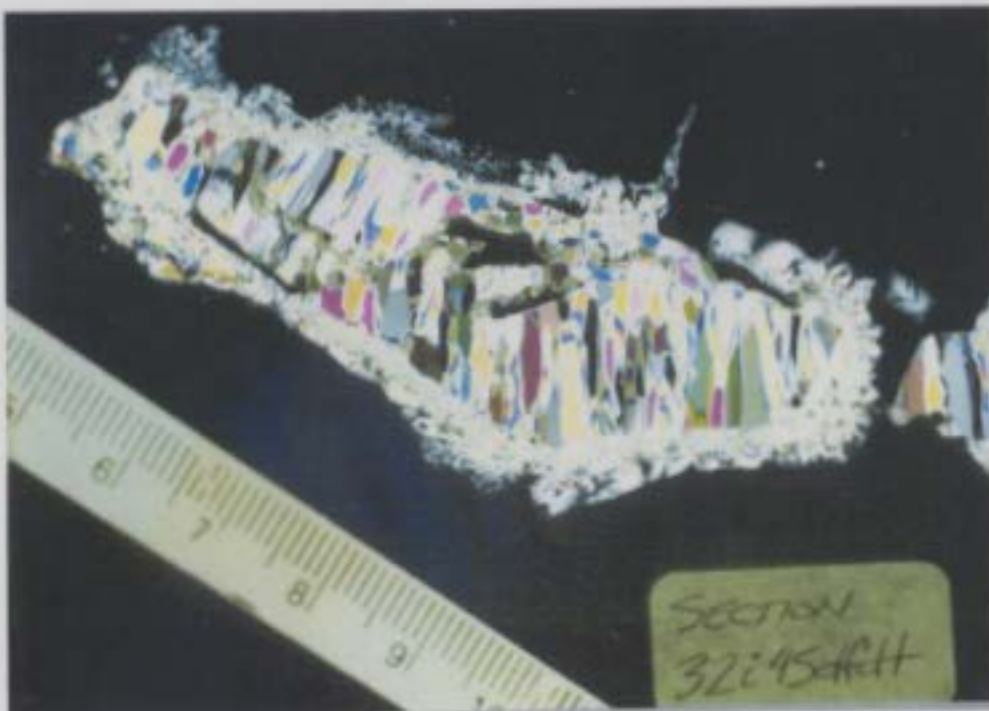


Figure 2: Section ICESTR32i45dfd



Figure 3: Section ICESTR32iiptdt

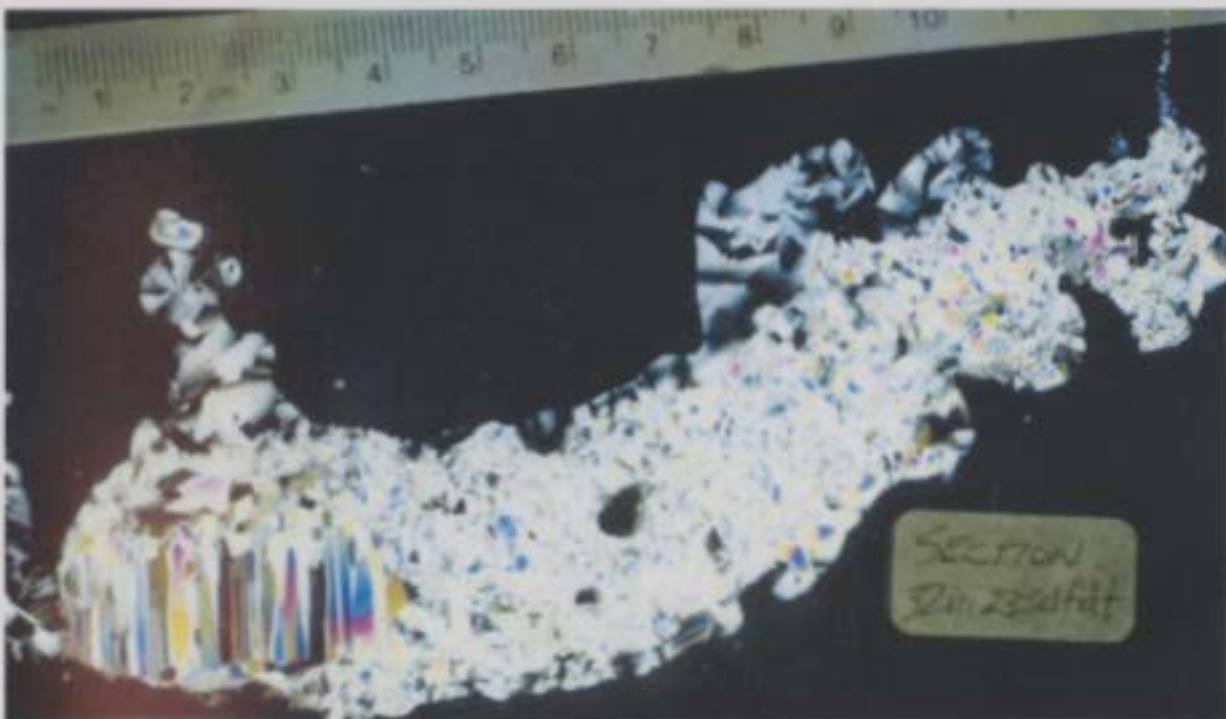


Figure 4: Section ICESTR32iii235dfdt



Figure 5: Section ICESTR32iv270dfdt

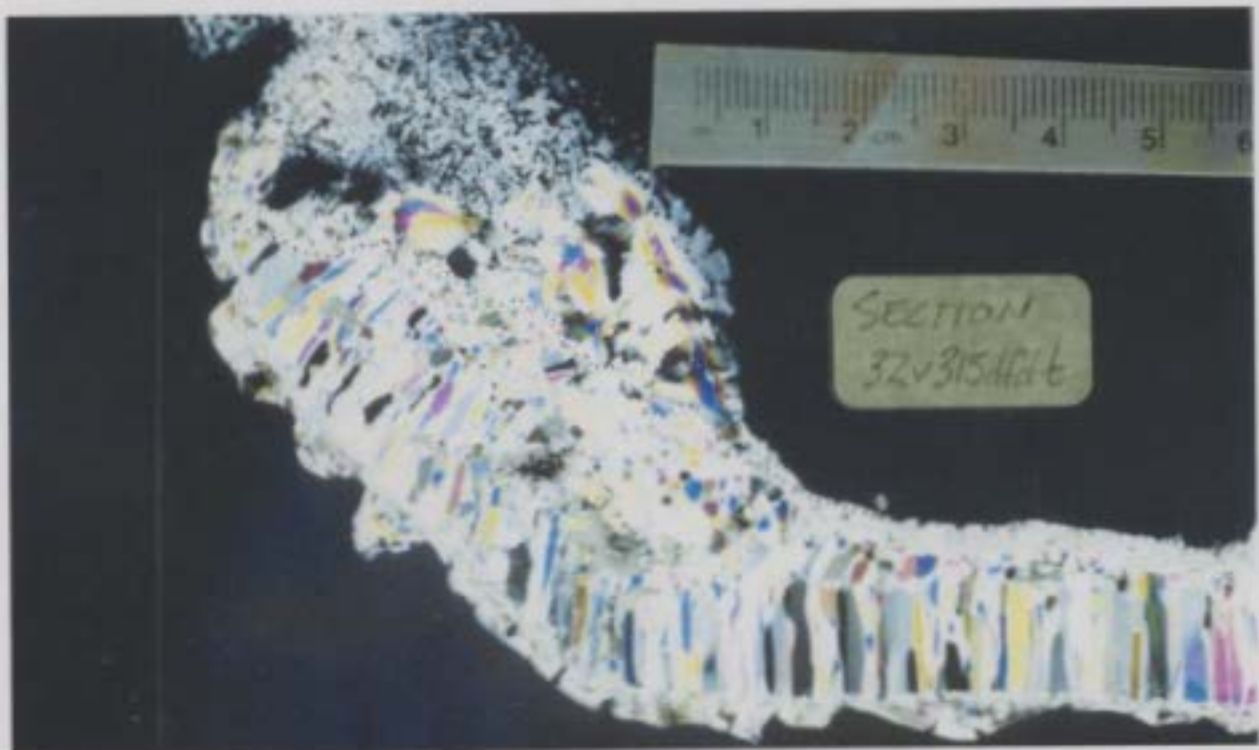


Figure 6: Section ICESTR32v315dfdt

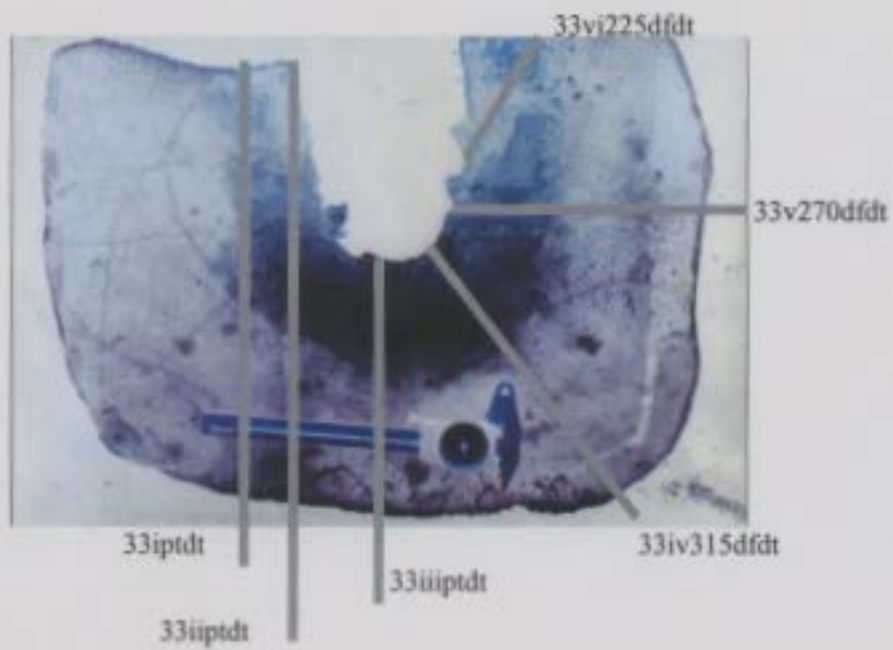


Figure 7: Section location outline - ICESTR33.



Figure 8: Section ICESTR33iptdt



Figure 9: Section ICESTR33iiptdt

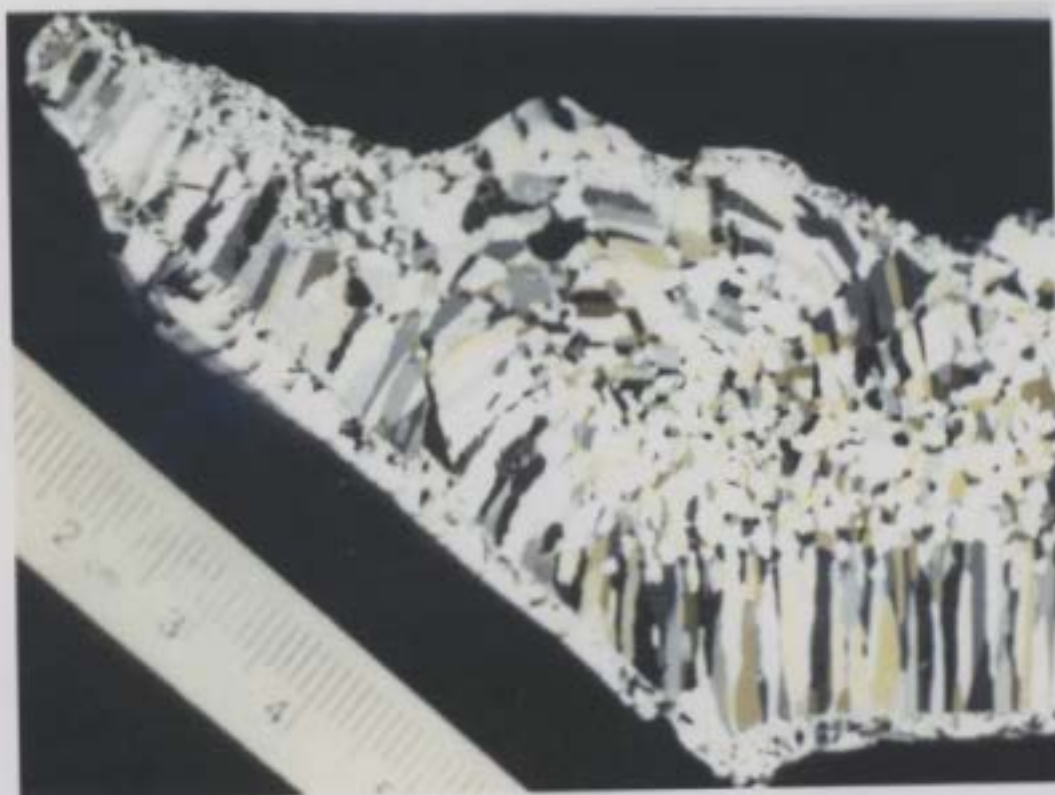


Figure 10: Section ICESTR33iiiptdt



Figure 11: Section ICESTR33iv315dfdt



Figure 12: Section ICESTR33v270dfdt



Figure 13: Section ICESTR33iv225dfdt

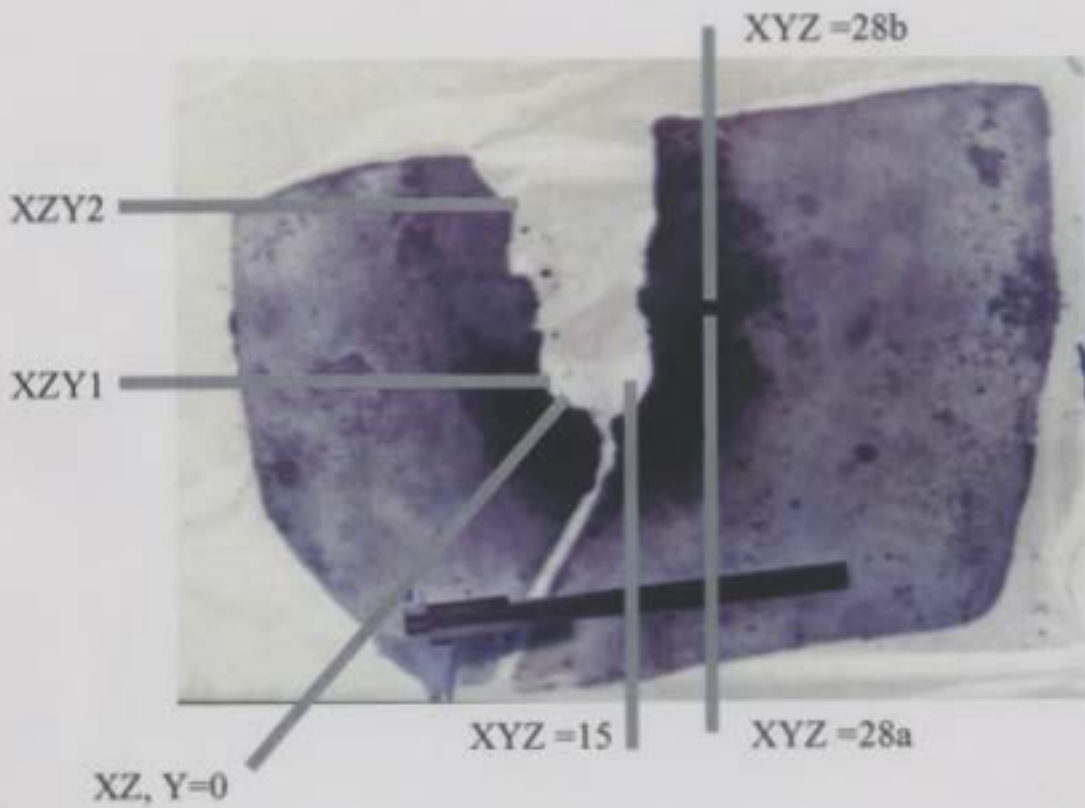


Figure 14: Section locations for ICESTR34



Figure 15: Section ICESTR34 XZ, Y=0

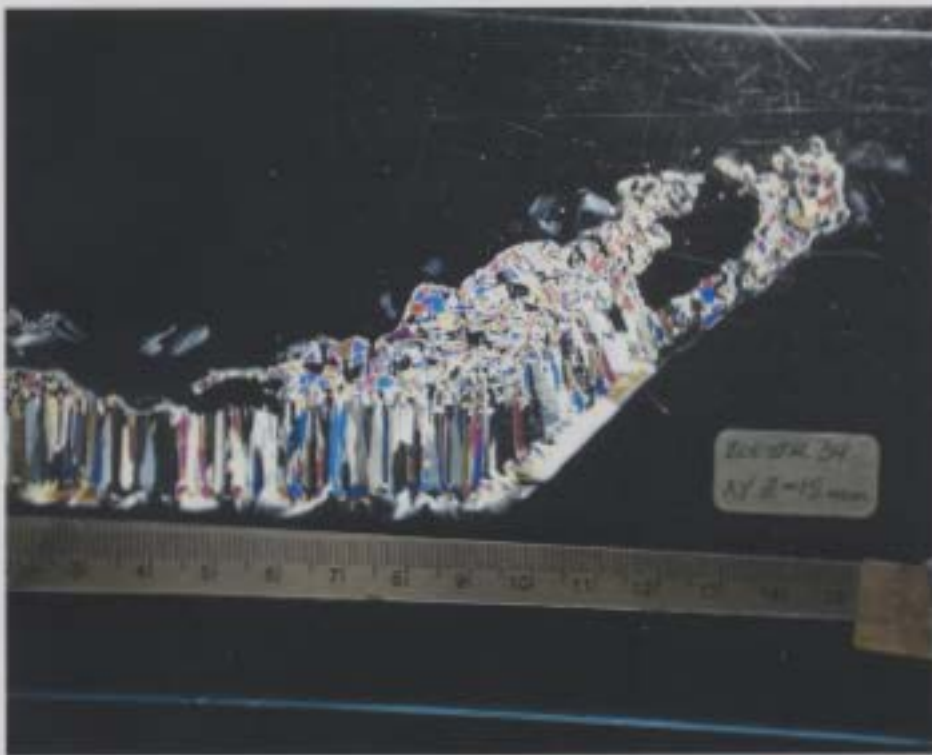


Figure 16: Section ICESTR34 XY, Z=15



Figure 17: Section ICESTR34 XY, Z=28a

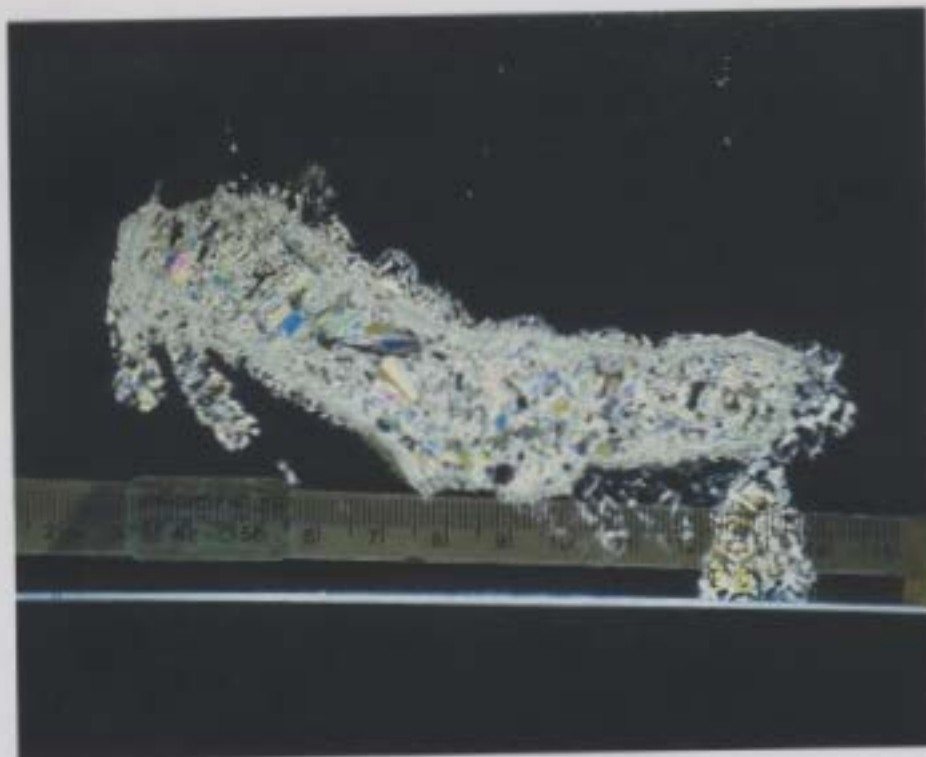


Figure 18: Section ICESTR34 XY, Z=28b

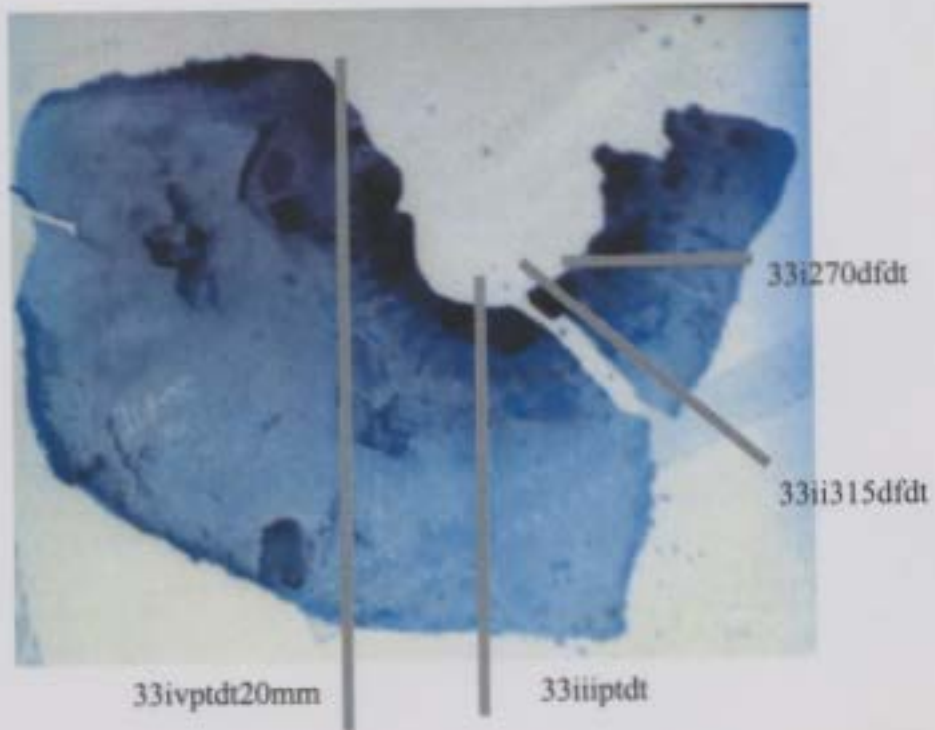


Figure 19: Section locations for ICESTR35



Figure 20: Section ICESTR35i270dfd



Figure 21: Section ICESTR35ii315dfdt



Figure 22: Section ICESTR35iii1ptdt



Figure 23: Section ICESTR35ivptdt



